Journal of Medicinal Chemistry

pubs.acs.org/jmc

Article

Structure-Guided Design of Conformationally Constrained Cyclohexane Inhibitors of Severe Acute Respiratory Syndrome Coronavirus-2 3CL Protease

Chamandi S. Dampalla, Yunjeong Kim, Naemi Bickmeier, Athri D. Rathnayake, Harry Nhat Nguyen, Jian Zheng, Maithri M. Kashipathy, Matthew A. Baird, Kevin P. Battaile, Scott Lovell, Stanley Perlman, Kyeong-Ok Chang,* and William C. Groutas*

Cite This: https://doi.org/10.1021/acs.jmedchem.1c00319

Read Online

ACCESS | Metrics & More | Article Recommendations | Supporting Information

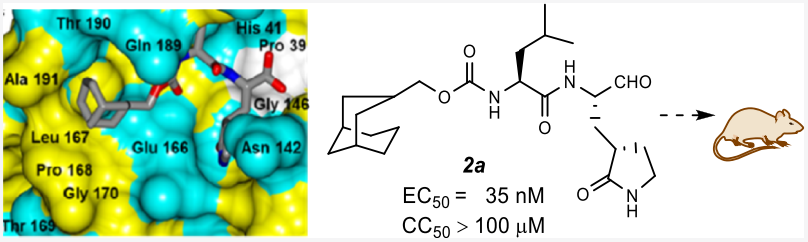

ABSTRACT: A series of nondeuterated and deuterated dipeptidyl aldehyde and masked aldehyde inhibitors that incorporate in their structure a conformationally constrained cyclohexane moiety was synthesized and found to potently inhibit severe acute respiratory syndrome coronavirus-2 3CL protease in biochemical and cell-based assays. Several of the inhibitors were also found to be nanomolar inhibitors of Middle East respiratory syndrome coronavirus 3CL protease. The corresponding latent aldehyde bisulfite adducts were found to be equipotent to the precursor aldehydes. High-resolution cocrystal structures confirmed the mechanism of action and illuminated the structural determinants involved in binding. The spatial disposition of the compounds disclosed herein provides an effective means of accessing new chemical space and optimizing pharmacological activity. The cellular permeability of the identified inhibitors and lack of cytotoxicity warrant their advancement as potential therapeutics for COVID-19.

INTRODUCTION

Coronaviruses are enveloped, positive-sense, single-stranded RNA viruses that belong to the family *Coronaviridae*.[1] Among human coronaviruses, several strains (229E, NL63, OC43, and KHU1) are the cause of mild upper respiratory infections; however, a few coronaviruses have emerged from animals that cause severe respiratory disease, including severe acute respiratory syndrome coronavirus (SARS-CoV), Middle East respiratory syndrome coronavirus (MERS-CoV), and SARS-CoV-2.[2] Of particular concern is SARS-CoV-2, the highly pathogenic causative agent of COVID-19 which is associated with high infectivity and is a significant threat to public health worldwide.[3,4] The problem is further compounded by the current lack of effective vaccines or small molecule therapeutics for the treatment of SARS-CoV-2 infections, underscoring the urgent and dire need for the development of prophylactic and therapeutic countermeasures to combat infections by pathogenic coronaviruses.[5−7]

The SARS-CoV-2 genome is large(∼30 kb) and similar to the genomes of SARS-CoV and MERS-CoV (∼80 and ∼50% sequence identity, respectively). It contains two open reading frames (ORF1a and ORF1b) and encodes multiple structural and nonstructural proteins.[1] Translation of the genomic mRNA of ORF1a yields a polyprotein (pp1a), while a second polyprotein (pp1ab) is the product of a ribosomal frameshift that joins ORF1a together with ORF1b. The two polyproteins are processed by a 3C-like protease (3CLpro, also referred to as main protease, M^{pro}) (11 cleavage sites) and a papain-like cysteine protease (PLpro), resulting in 16 mature nonstructural proteins which are involved in the replication−transcription complex. The two proteases are essential for viral replication, making them attractive targets for therapeutic intervention.[8−15]

SARS-CoV-2 3CLpro is a homodimer with a catalytic Cys−His dyad (Cys145−His41) and an extended binding cleft. Substrate specificity profiling studies[12,13] have shown that the protease displays a strong preference for a −Y−Z−Leu−Gln−X sequence, where X is a small amino acid, Y is a hydrophobic

Received: February 20, 2021

amino acid, and Z is solvent-exposed and fairly diverse (V/T/K), corresponding to the amino acid residues $-P_4-P_3-P_2-P_1-P_1'$-of a substrate or inhibitor.[16] Cleavage is at the P_1-P_1' scissile bond. The 3D structure of SARS-CoV-2 3CLpro is similar to that of SARS-CoV 3CLpro; however, the S_2 subsite of SARS-CoV-2 3CLpro displays considerable plasticity and can accommodate natural and unnatural amino acids with smaller side chains.[12] Similarly, the active-site topography of MERS-CoV 3CLpro closely resembles that of SARS-CoV-2 3CLpro.[17] High-resolution crystal structures with bound inhibitors have been determined, enabling the use of structure-guided approaches in the design of inhibitors. In continuing our foray in this area,[17−19] we report herein the results of preliminary studies related to the inhibition of SARS-CoV-2 protease by a series of inhibitors (I) (Scheme 1) that incorporate in their structure a conformationally constrained cyclohexane moiety envisaged to exploit new chemical space and to optimally engage in favorable binding interactions with the active site of the protease. Furthermore, several deuterated variants of the inhibitor were also synthesized to potentially improve the PK properties and ancillary parameters of the inhibitors.[20−22]

Scheme 1. Synthesis of Inhibitors 2(a−o) and 3(a−o)

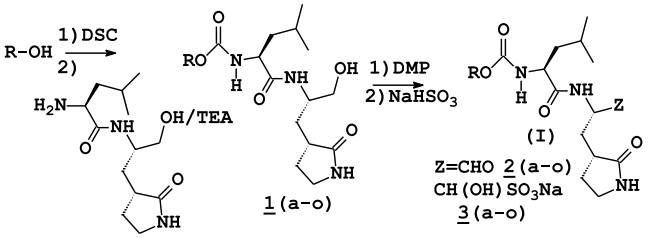

RESULTS AND DISCUSSION

Inhibitor Design Rationale. The design of inhibitor (I) (Scheme 1) included the use of a P_1 glutamine surrogate residue and a P_2 Leu residue as recognition elements congruent with the substrate specificity of the protease,[12,13] as well as an aldehyde warhead or a latent aldehyde bisulfite adduct. The design of the inhibitor (I) was further abetted by insights gained from examining the available X-ray crystal structures of the protease with inhibitors[12,13,17] and the results of recent studies with cyclohexyl-derived inhibitors with demonstrated efficacy in a mouse model of MERS-CoV-2 infection and potent inhibition against SARS-CoV-2 3CL protease.[17]

Chemistry. The synthesis of inhibitors **2(a−o)** and **3(a−o)** was readily accomplished by activating the precursor primary or secondary alcohol inputs (Scheme 2) with *N,N′*-disuccinimidyl carbonate[23] and coupling the mixed carbonate with the readily accessible Leu−Gln surrogate amino alcohol to yield alcohol product **1** which was oxidized with Dess-Martin periodinane to generate the corresponding aldehyde (Scheme 1, Z = CHO **2**). The aldehydes were subsequently converted to the corresponding bisulfite adducts (Scheme 1, Z = $CH(OH)SO_3Na$ **3**).[24]

Biochemical Studies. The inhibitory activity of compounds **2−3 (a−o)** against SARS-CoV-2 3CL protease[17,25] and their activity in a cell-based system were determined as described in the Experimental Section. The IC_{50} values, EC_{50} values for two representative inhibitors (**2a**/**3a**), and the CC_{50} values in Huh-7, CRFK, or CCL1 cells[17,25] are summarized in Table 1, and they are the average of at least two determinations. The inhibitory activity of compounds **2a**/**3a**, **2f**/**3f**, and **2k**/**3k** against MERS-CoV 3CL protease was also determined as described previously,[17,18,25] and the IC_{50} values are listed in Table 2.

It is clearly evident from the results shown in Table 1 that the synthesized compounds display high potency in biochemical assays, with most IC_{50} values in the sub-micromolar range. Furthermore, the inhibitors were found to be devoid of cytotoxicity and the safety index (SI), defined as the CC_{50}/IC_{50} ratio, ranged between ∼78 and 1110. The potency of deuterated variants **2b**/**3b** decreased ∼1.6-fold (aldehydes) and ∼1.7-fold (bisulfite adducts) as compared to the respective nondeuterated compounds **2a**/**3a** and remained essentially the same in the case of nondeuterated **2n**/**3n** and deuterated **2o**/**3o** inhibitors, respectively. A change in geometry from a cyclohexene (**2e**/**3e**) to a cyclohexane (**2f**/**3f**) resulted in a two- to threefold increase in potency. The approximately fivefold decrease in potency of compounds **2n**/**3n** compared to **2k**/**3k** presumably reflects the inimical effect on potency of the 3° hydroxyl group. Importantly, the EC_{50} values of two representative inhibitors (**2a**/**3a**) against SARS-CoV-2 in Vero E6 cells were found to be ∼4.6-fold lower (EC_{50} 0.035 and 0.032 μM, respectively) than the corresponding IC_{50} values, and the selectivity indices of compounds **2a**/**3a** were very high (2857 and 3125, respectively). The significance of these findings was further augmented by the notable inhibition of MERS-CoV 3CL protease by a select number of inhibitors (Table 2, compounds **2a**/**3a**, **2f**/**3f**, and **2k**/**3k**), demonstrat-

Scheme 2. Alcohol Inputs (a−o)

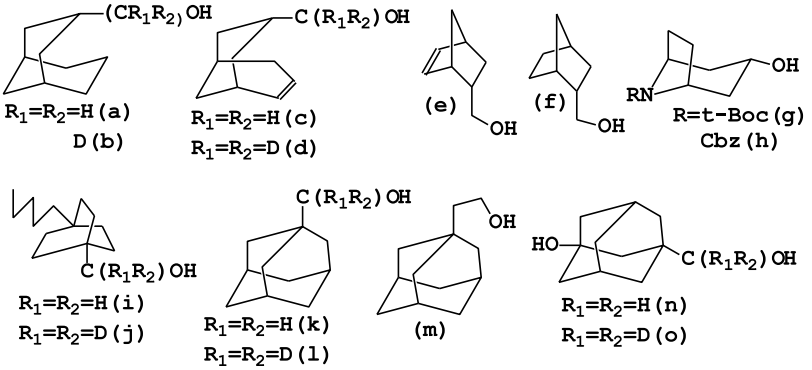

https://doi.org/10.1021/acs.jmedchem.1c00319
J. Med. Chem. XXXX, XXX, XXX−XXX

Table 1. IC_{50} and CC_{50} Values of SARS-CoV-2 3CLpro Inhibitors 2−3 (a−o)

compound	IC_{50} (μM)	CC_{50} (μM)	compound	IC50 (μM)	CC_{50} (μM)
2a	0.18 ± 0.03[a]	>100	**3h**	0.37 ± 0.03	>100
3a	0.17 ± 0.02[a]	>100	**2i**	0.27 ± 0.02	21 ± 1
2b	0.29 ± 0.05	>100	**3i**	0.30 ± 0.02	21 ± 3
3b	0.29 ± 0.01	>100	**2j**	0.31 ± 0.03	20 ± 3
2c	0.31 ± 0.06	>100	**3j**	0.31 ± 0.06	23 ± 1
3c	0.26 ± 0.05	>100	**2k**	0.18 ± 0.04	>100
2d	0.28 ± 0.08	>100	**3k**	0.15 ± 0.04	>100
3d	0.30 ± 0.03	>100	**2l**	0.29 ± 0.04	>100
2e	0.26 ± 0.05	>100	**3l**	0.27 ± 0.04	>100
3e	0.28 ± 0.03	>100	**2m**	0.27 ± 0.02	>100
2f	0.14 ± 0.02	>100	**3m**	0.25 ± 0.04	>100
3f	0.10 ± 0.01	>100	**2n**	0.82 ± 0.19	>100
2g	1.90 ± 0.14	>100	**3n**	1.03 ± 0.24	>100
3g	1.71 ± 0.16	>100	**2o**	0.74 ± 0.26	>100
2h	0.39 ± 0.02	>100	**3o**	0.78 ± 0.18	>100

[a]The EC_{50} values for inhibitors **2a** and **3a** against SARS-CoV-2 in Vero E6 cells were 0.035 ± 0.001 and 0.032 ± 0.001 μM, respectively.

Table 2. IC_{50} Values of MERS-CoV 3CLpro Inhibitors 2a/3a, 2f/3f, and 2k/3k

compound	IC_{50} (μM)
2a	0.052 ± 0.001
3a	0.049 ± 0.002
2f	0.063 ± 0.003
3f	0.058 ± 0.002
2k	0.055 ± 0.002
3k	0.053 ± 0.003

ing the broad spectrum of antiviral activity displayed by this series of compounds.

Emergence of viral resistance to antiviral drugs is a major concern. We previously reported that GC376 has a high barrier to resistance to feline infectious peritonitis virus (FIPV) in cell culture and naturally infected animals with long-term treatment.[18] We also examined several compounds similar to the series in this report for emergence of viral resistance by serial passaging FIPV in the presence of each compound in cell culture. The EC_{50} values of the compounds did not increase at up to 10 passage number, and the 3CLpro of viruses passaged with each compound has the same sequence as mock-passaged viruses. These results suggest that this series of compounds have a high barrier to resistance.

X-ray Crystallography Studies. In order to elucidate the mechanism of action of the inhibitors and identify the structural determinants associated with the binding of inhibitors to the active site of SARS-CoV-2 3CL protease, high-resolution cocrystal structures were determined for inhibitors **2a**, **3b**, **2f**, **2k**, **3c**, **3d** and **3e**. The structure of SARS-CoV-2 3CLpro in complex with compound **2a** contained a prominent difference in electron density consistent with the inhibitor covalently bound to Cys145 in each subunit (Figure 1A,B). The electron density was consistent with the inhibitor aldehyde carbon covalently bound to the Sγ atom of the catalytic Cys145 residue and the formation of a tetrahedral hemithioacetal, confirming the mechanism of action. Both the

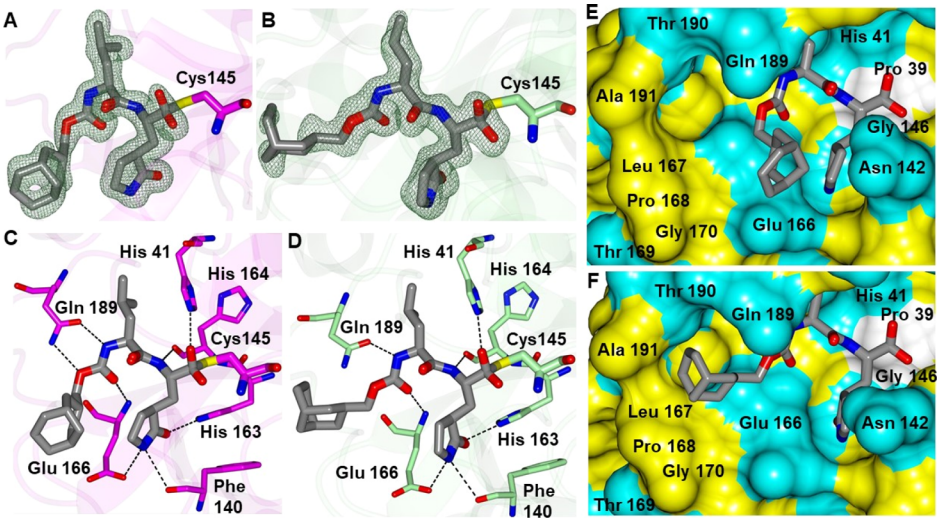

Figure 1. Binding mode of **2a** (gray) with SARS-CoV-2 3CLpro associated with subunit A (A,C) and subunit B (B,D). Fo−Fc polder omit map (green mesh) contoured at 3σ (A,B). Hydrogen bond interactions (dashed lines) (C,D). Surface representations showing the orientation of **2a** in subunit A (E) and subunit B (F) near the S_4 subsite of SARS-CoV-2 3CLpro with neighboring residues colored yellow (nonpolar), cyan (polar), and white (weakly polar).

https://doi.org/10.1021/acs.jmedchem.1c00319
J. Med. Chem. XXXX, XXX, XXX−XXX

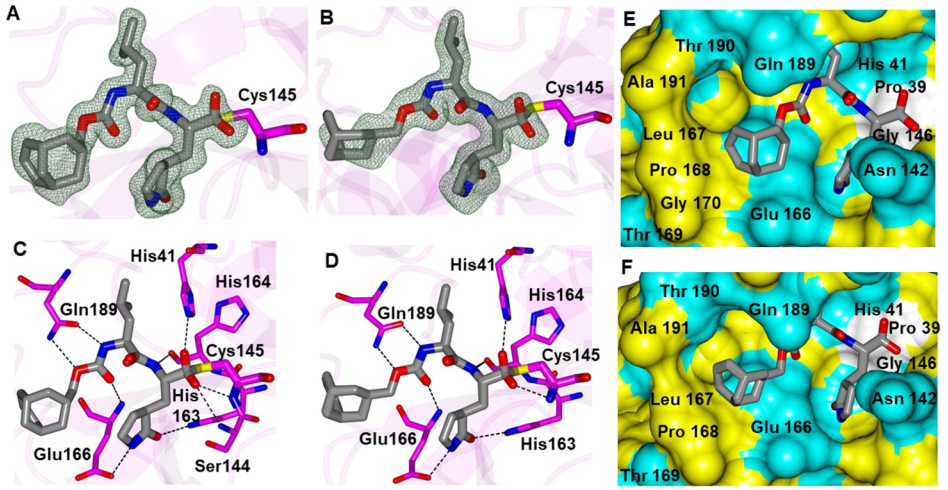

Figure 2. Binding mode of **3c** (A,B,E) and its deuterated analogue **3d** (C,D,F) with SARS-CoV-2 3CLpro. Fo−Fc polder omit map (green mesh) contoured at 3σ (A,B). Hydrogen bond interactions (dashed lines) (C,D). surface representation showing the orientation of **3c** (E) and **3d** (F) near the S_4 subsite of SARS-CoV-2 3CLpro with neighboring residues colored yellow (nonpolar), cyan (polar), and white (weakly polar).

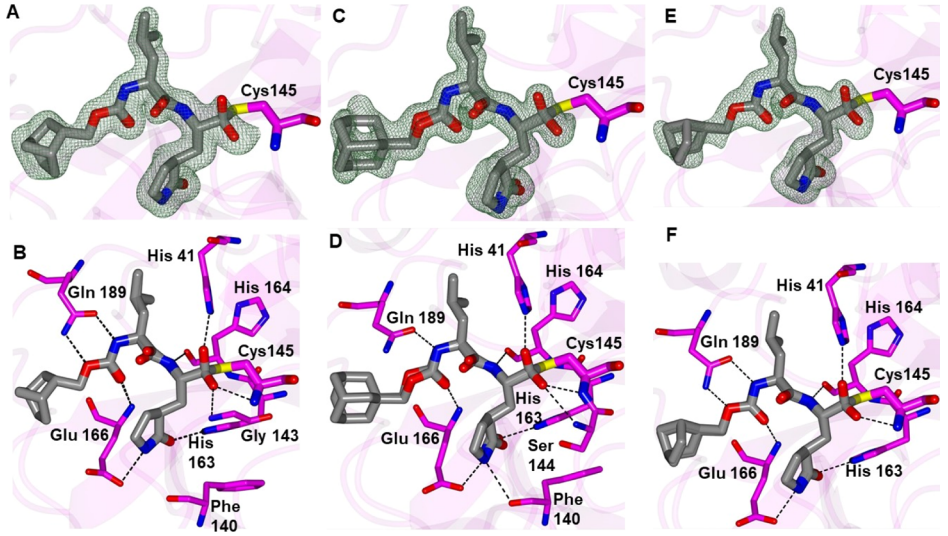

Figure 3. Binding mode of **2f** (A,B), **2k** (C,D), and **3e** (E,F) with SARS-CoV-2 3CLpro. Fo−Fc polder omit map (green mesh) contoured at 3σ (A,C,E). Hydrogen bond interactions (dashed lines) (B,D,F).

R- and S-enantiomers were observed at the newly formed stereocenter, and each enantiomer was modeled with 0.5 occupancy and was observed for all structures described here. Interestingly, **2a** adopts two conformations in which the bicyclic ring is projected away from the S_4 subsite in subunit A and is positioned in the S_4 subsite in subunit B. The inhibitor engages in multiple favorable binding interactions with the enzyme, including direct hydrogen bond interactions with His163 and Glu166 (γ-lactam C═O and N−H, respectively), His41, Phe140, Ser144, His164, and Gln189 (Figure 1C,D). The isobutyl side chain of Leu is ensconced in the hydrophobic S_2 pocket, and the γ-lactam ring of the P_1 Gln surrogate is nestled in the S_1 subsite forming hydrogen bonds with His163 and Glu166. In addition, the lipophilic bicyclic ring in subunit A is directed toward the surface, whereas in subunit B, it is anchored in the vicinity of the hydrophobic S_4 pocket that is lined by Ala191, Leu197, and Pro168 (Figure 1E,F). It should be noted that the 11 sites in the pp1a and pp1ab polyproteins cleaved by the protease are all characterized by the presence of a P_1 Gln residue, which is conserved in all known coronavirus 3CLpro cleavage sites. Interestingly, the deuterated analogue **3b** adopts the same binding mode and superimposes nearly identical to **2a**, as shown in Figure S1. The root mean square deviation (RMSD) between the Cα atoms of **2a** and **3b** was 0.27 Å for 594 residues aligned.

Likewise, the structure of **3c** shows similar binding mode properties to those observed for **2a** (Figure 2A,C,E). The inhibitor engages in multiple favorable binding interactions with the enzyme, including direct hydrogen bond interactions with His163 and Glu166 (γ-lactam C═O and N−H, respectively), His41, Ser144, His164, and Gln189. The bicyclic ring is oriented within the hydrophobic S_4 pocket, in both subunits. Likewise, the structure of SARS-CoV-2 3CL protease with deuterated inhibitor **3d** adopts a very similar binding mode (Figure 2C,D,F). The main difference is that the electron density for **3c** is the most consistent with an axial conformation of the carbon atom attached to the bicyclic ring, whereas **3d** appears to adopt an equatorial orientation (Figure S2). The structures are very similar overall, and the

https://doi.org/10.1021/acs.jmedchem.1c00319
J. Med. Chem. XXXX, XXX, XXX−XXX

superposition yielded an RMSD between the Cα atoms of 0.25 Å for 596 residues aligned.

Similarly, inhibitors **2f**, **2k**, and **3e** in complex with SARS-CoV-2 were found to adopt similar binding modes in the active site of the protease, as shown in Figures 3 and S3. Collectively, the bicyclic rings of the inhibitors span a relatively small region in the active site and cover a space of approximately 6.3 Å (Figure 4). As such, these cocrystal structures provide valuable insights for further structure-guided multiparameter optimization.

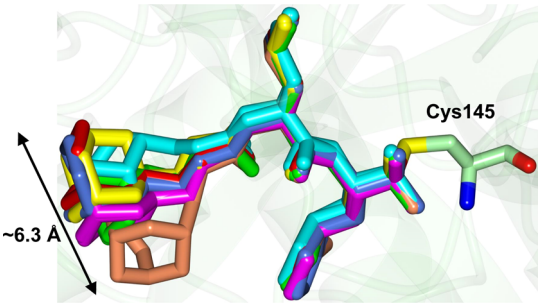

Figure 4. Superposition of all seven inhibitor-bound structures **2a** (red), **3b** (blue), **2f** (cyan), **2k** (yellow), **3c** (coral), **3d** (magenta), and **3e** (green). The bicyclic rings cover a space of approximately 6.3 Å in the S_4 subsite.

CONCLUSIONS

Given the major clinical importance associated with the SARS-CoV-2 pandemic and the current paucity of effective countermeasures, the results of the studies described herein can serve as a launching pad for conducting further preclinical studies. Most of the compounds exhibited high potency in biochemical assays and, for two of the compounds tested, in cellular assays. Furthermore, members of this series were also found to potently inhibit MERS-CoV 3CL protease, suggesting that the compounds can be developed into broad-spectrum antivirals. Since there are no known human proteases that have a primary substrate specificity P_1 residue, that is, Gln, these inhibitors could also display high selectivity and diminished off-target effects. Furthermore, the utilization of an aldehyde warhead, or a latent aldehyde functionality that can rapidly generate the aldehyde *in vivo*, in the design of transition state inhibitors is advantageous for several reasons, including rapid engagement with the target, leading to the reversible formation of a covalent adduct. The high reactivity of aldehydes is generally viewed as a toxicity alert; however, the safety indices for most of the compounds reported herein were found to be high. Indeed, a number of pharmaceuticals that incorporate in their structure an aldehyde functionality are currently in clinical use and, furthermore, toxicity arising from the presence of the aldehyde is context-specific,[26] as is presumably the case here. Finally, the present study also sought to exploit the kinetic isotope effect associated with the H/D bioisosteric replacement[27,28] in order to dampen oxidative metabolism at the $-CH_2O-$ metabolic soft spot in the inhibitors,[29] as well as to reduce toxicity. Thus, the availability of equipotent deuterated analogues that display improved PK characteristics enhances further the significance of the results reported herein. Evaluation of a select number of inhibitors in a mouse model of SARS-CoV-2 infection is in progress, and the results will be reported in due course. In conclusion, a series of potent transition state inhibitors of SARS-CoV-2 3CL protease that incorporate in their structures a conformationally constrained cyclohexyl moiety is reported.

EXPERIMENTAL SECTION

General. Reagents and dry solvents were purchased from various chemical suppliers (Sigma-Aldrich, Acros Organics, Chem-Impex, TCI America, Oakwood chemical, APExBIO, Cambridge Isotopes, Alpha Aesar, Fisher, and Advanced Chemblocks) and were used as obtained. Silica gel (230−450 mesh) used for flash chromatography was purchased from Sorbent Technologies (Atlanta, GA). Thin layer chromatography was performed using Analtech silica gel plates. Visualization was accomplished using UV light and/or iodine. Nuclear magnetic resonance (NMR) spectra were recorded in $CDCl_3$ or dimethyl sulfoxide (DMSO)-d_6 using a Varian XL-400 spectrometer. High-resolution mass spectrometry (HRMS) was performed at the Wichita State University mass spectrometry laboratory using an Orbitrap Velos Pro mass spectrometer (ThermoFisher, Waltham, MA) equipped with an electrospray ion source. The purity of all final compounds was >95% as evidenced by NMR analysis.

SYNTHESIS OF COMPOUNDS

Preparation of Compounds 1(a−o). *General Procedure.* To a solution of alcohol (1 equiv) (Scheme 2) in anhydrous acetonitrile (10 mL/g alcohol) was added DSC (1.2 equiv) and TEA (3.0 equiv), and the reaction mixture was stirred for 4 h at room temperature. The solvent was removed *in vacuo*, and the residue was dissolved in ethyl acetate (40 mL/g alcohol). The organic phase was washed with saturated aqueous $NaHCO_3$ (2 × 20 mL/g alcohol), followed by brine (20 mL/g alcohol). The organic layers were combined and dried over anhydrous Na_2SO_4, filtered, and concentrated *in vacuo* to yield the mixed carbonate which was used in the next step without further purification.

To a solution of Leu−Gln surrogate amino alcohol (1.0 equiv) in dry methylene chloride (10 mL/g amino alcohol) was added TEA (1.5 equiv), and the reaction mixture was stirred for 20 min at room temperature (solution 1). In a separate flask, the mixed carbonate was dissolved in dry methylene chloride (10 mL/g carbonate) (solution 2). Solution 1 was added to solution 2, and the reaction mixture was stirred for 3 h at room temperature. Methylene chloride was added to the organic phase (40 mL/g carbonate) and then washed with saturated aqueous $NaHCO_3$ (2 × 20 mL/g alcohol), followed by brine (20 mL/g alcohol). The organic phase was dried over anhydrous Na_2SO_4, filtered, and concentrated *in vacuo*. The resultant crude product was purified by flash chromatography (hexane/ethyl acetate) to yield dipeptidyl alcohol **1** as a white solid.

*((1R,5S)-Bicyclo[3.3.1]nonan-3-yl)methyl((S)-1-(((S)-1-hydroxy-3-((S)-2-oxopyrrolidin-3-yl)propan-2-yl)amino)-4-methyl-1-oxopentan-2-yl)carbamate (**1a**).* Yield (35%); ^{1}H NMR (400 MHz, $CDCl_3$): δ 7.75 (d, *J* = 7.2 Hz, 1H), 6.24 (s, 1H), 5.31 (d, *J* = 9.1 Hz, 1H), 4.29−4.10 (m, 1H), 4.10−3.93 (m, 1H), 3.89 (d, *J* = 6.3 Hz, 1H), 3.71−3.54 (m, 2H), 3.48 (d, *J* = 2.0 Hz, 1H), 3.39−3.27 (m, 2H), 2.55−2.25 (m, 3H), 2.03 (d, *J* = 11.9 Hz, 3H), 1.96−1.77 (m, 4H), 1.77−1.57 (m, 4H), 1.57−1.44 (m, 1H), 1.37 (d, *J* = 9.5 Hz, 4H), 1.27−1.15 (m, 1H), 1.09 (dd, *J* = 12.8, 2.6 Hz, 1H), 0.95 (d, *J* = 6.3 Hz, 6H), 0.91−0.80 (m, 2H).

*((1R,3S,5S)-Bicyclo[3.3.1]nonan-3-yl)methyl-d_2((S)-1-(((S)-1-hydroxy-3-((S)-2-oxopyrrolidin-3-yl)propan-2-yl)amino)-4-methyl-1-oxopentan-2-yl)carbamate (**1b**).* Yield (36%); ^{1}H NMR (400 MHz, $CDCl_3$): δ 7.77 (d, *J* = 7.1 Hz, 1H), 6.25 (s,

https://doi.org/10.1021/acs.jmedchem.1c00319
J. Med. Chem. XXXX, XXX, XXX−XXX

1H), 5.30 (s, 1H), 4.27−3.93 (m, 2H), 3.69−3.55 (m, 2H), 3.39−3.32 (m, 2H), 2.53−2.35 (m, 2H), 2.09−1.96 (m, 4H), 1.96−1.77 (m, 3H), 1.77−1.58 (m, 5H), 1.58−1.47 (m, 1H), 1.45−1.30 (m, 5H), 1.09 (d, J = 12.8 Hz, 1H), 0.95 (d, J = 6.4 Hz, 6H), 0.88 (d, J = 13.1 Hz, 2H).

*((1S,5R)-Bicyclo[3.3.1]non-6-en-3-yl)methyl((S)-1-(((S)-1-hydroxy-3-((S)-2-oxopyrrolidin-3-yl)propan-2-yl)amino)-4-methyl-1-oxopentan-2-yl)carbamate (**1c**).* Yield (35%). ^{1}H NMR (400 MHz, $CDCl_3$): δ 7.74 (s, 1H), 5.98 (s, 1H), 5.85 (t, J = 8.0 Hz, 1H), 5.58 (t, J = 9.7 Hz, 1H), 5.19 (s, 1H), 4.21−4.16 (m, 1H), 4.07 (d, J = 2.5 Hz, 2H), 4.02−3.95 (m, 1H), 3.68−3.56 (m, 2H), 3.38−3.32 (m, 2H), 2.50−2.36 (m, 2H), 2.36−2.31 (m, 1H), 2.31−2.25 (m, 2H), 2.17−2.09 (m, 1H), 2.03−1.95 (m, 1H), 1.95−1.87 (m, 1H), 1.87−1.81 (m, 2H), 1.81−1.73 (m, 2H), 1.73−1.59 (m, 3H), 1.56−1.46 (m, 2H), 1.46−1.35 (m, 2H), 0.95 (d, J = 6.5 Hz, 6H).

*((1S,3S,5R)-Bicyclo[3.3.1]non-6-en-3-yl)methyl-d_2((S)-1-(((S)-1-hydroxy-3-((S)-2-oxopyrrolidin-3-yl)propan-2-yl)amino)-4-methyl-1-oxopentan-2-yl)carbamate (**1d**).* Yield (36%). ^{1}H NMR (400 MHz, $CDCl_3$): δ 7.72 (s, 1H), 6.04 (s, 1H), 5.85 (t, J = 8.1 Hz, 1H), 5.62−5.55 (m, 1H), 5.20 (s, 1H), 4.23−4.15 (m, 1H), 4.02−3.93 (m, 1H), 3.68−3.54 (m, 2H), 3.39−3.33 (m, 2H), 2.49−2.31 (m, 3H), 2.30−2.26 (m, 1H), 2.16−2.09 (m, 1H), 2.03−1.95 (m, 2H), 1.93−1.78 (m, 4H), 1.78−1.59 (m, 4H), 1.59−1.46 (m, 2H), 1.46−1.35 (m, 2H), 0.95 (d, J = 6.5 Hz, 6H).

*Bicyclo[2.2.1]hept-5-en-2-ylmethyl((S)-1-(((S)-1-hydroxy-3-((S)-2-oxopyrrolidin-3-yl)propan-2-yl)amino)-4-methyl-1-oxopentan-2-yl)carbamate (**1e**).* Yield (44%). ^{1}H NMR (400 MHz, $CDCl_3$): δ 7.74 (s, 1H), 6.38 (s, 1H), 6.14 (dd, J = 5.7, 3.0 Hz, 1H), 5.93 (dd, J = 5.8, 2.9 Hz, 1H), 5.41−5.32 (m, 1H), 4.27−4.19 (m, 1H), 4.19−4.07 (m, 1H), 4.06−3.89 (m, 1H), 3.88−3.80 (m, 1H), 3.69−3.53 (m, 3H), 3.35 (dd, J = 10.6, 4.2 Hz, 2H), 2.87−2.77 (m, 2H), 2.52−2.34 (m, 2H), 2.10−1.87 (m, 1H), 1.87−1.77 (m, 1H), 1.77−1.57 (m, 3H), 1.57−1.47 (m, 1H), 1.47−1.40 (m, 1H), 1.37−1.18 (m, 1H), 1.18−1.10 (m, 1H), 0.96 (d, J = 6.5 Hz, 6H), 0.53 (ddd, J = 11.7, 4.5, 2.6 Hz, 1H).

*Bicyclo[2.2.1]heptan-2-ylmethyl((S)-1-(((S)-1-hydroxy-3-((S)-2-oxopyrrolidin-3-yl)propan-2-yl)amino)-4-methyl-1-oxopentan-2-yl)carbamate (**1f**).* Yield (44%). ^{1}H NMR (400 MHz, $CDCl_3$): δ 7.73 (s, 1H), 6.30 (s, 1H), 5.30 (s, 1H), 4.30−4.15 (m, 1H), 4.15−4.04 (m, 1H), 4.04−3.95 (m, 1H), 3.95−3.85 (m, 1H), 3.78 (d, J = 8.0 Hz, 1H), 3.71−3.52 (m, 2H), 3.39−3.32 (m, 2H), 2.48−2.36 (m, 2H), 2.24−2.17 (m, 1H), 2.17−1.96 (m, 1H), 1.97−1.75 (m, 1H), 1.75−1.56 (m, 3H), 1.56−1.41 (m, 3H), 1.41−1.21 (m, 3H), 1.21−0.99 (m, 3H), 0.95 (d, J = 6.4 Hz, 6H), 0.66 (dd, J = 12.6, 5.1 Hz, 1H).

*tert-Butyl (1R,3s,5S)-3-((((S)-1-(((S)-1-Hydroxy-3-((S)-2-oxopyrrolidin-3-yl)propan-2-yl)amino)-4-methyl-1-oxopentan-2-yl)carbamoyl)oxy)-8-azabicyclo[3.2.1]octane-8-carboxylate (**1g**).* Yield (45%). ^{1}H NMR (400 MHz, $CDCl_3$): δ 7.85 (s, 1H), 6.29 (s, 1H), 5.31 (d, J = 9.3 Hz, 1H), 4.94 (s, 1H), 4.29−4.02 (m, 3H), 4.01−3.97 (m, 1H), 3.64−3.59 (m, 2H), 3.39−3.31 (m, 2H), 2.44−2.39 (m, 2H), 2.20−1.89 (m, 8H), 1.84 (dd, J = 11.3, 9.0 Hz, 1H), 1.76 (d, J = 15.2 Hz, 2H), 1.73−1.60 (m, 2H), 1.60−1.48 (m, 1H), 1.46 (s, 9H), 0.99−0.91 (m, 6H).

*Benzyl (1R,3s,5S)-3-((((S)-1-(((S)-1-hydroxy-3-((S)-2-oxopyrrolidin-3-yl)propan-2-yl)amino)-4-methyl-1-oxopentan-2-yl)carbamoyl)oxy)-8-azabicyclo[3.2.1]octane-8-carboxylate (**1h**).* Yield (49%). ^{1}H NMR (400 MHz, DMSO-d_6): δ 7.60−7.56 (m, 2H), 7.47−7.10 (m, 6H), 5.11 (d, J = 10.53 Hz, 2H), 5.02−4.88 (m, 1H), 4.83−4.61 (m, 1H), 4.30−4.15 (m, 2H), 4.05 (d, J = 7.11 Hz, 1H), 3.97−3.88 (m, 2H), 3.79−3.71 (m, 1H), 3.65−3.56 (m, 2H), 2.79−2.71 (m, 1H), 2.30−1.35 (m, 5H), 1.35−0.90 (m, 9H), 0.87 (td, J = 9.48, 8.02, 8.02 Hz, 6H).

*(4-Pentylbicyclo[2.2.2]octan-1-yl)methyl ((S)-1-(((S)-1-Hydroxy-3-((S)-2-oxopyrrolidin-3-yl)propan-2-yl)amino)-4-methyl-1-oxopentan-2-yl)carbamate (**1i**).* Yield (33%). ^{1}H NMR (400 MHz, DMSO-d_6): δ 7.63−7.45 (m, 1H), 7.09−6.97 (m, 2H), 6.94−4.71 (m, 2H), 4.69−4.57 (m, 5H), 2.90 (s, 1H), 2.78−2.70 (m, 1H), 1.95−1.87 (m, 5H), 1.32 (d, J = 7.74 Hz, 6H), 1.23−1.15 (m, 19H), 0.86 (dd, J = 13.86, 6.91 Hz, 6H).

*(4-Pentylbicyclo[2.2.2]octan-1-yl)methyl-d_2 ((S)-1-(((S)-1-hydroxy-3-((S)-2-oxopyrrolidin-3-yl)propan-2-yl)amino)-4-methyl-1-oxopentan-2-yl)carbamate (**1j**).* Yield (20%). ^{1}H NMR (400 MHz, DMSO-d_6): δ 7.62−7.47 (m, 1H), 7.10−6.97 (m, 2H), 6.97−4.75 (m, 2H), 4.69−4.59 (m, 3H), 2.92 (s, 1H), 2.78−2.76 (m, 1H), 1.95−1.87 (m, 5H), 1.39 (d, J = 7.74 Hz, 6H), 1.23−1.17 (m, 19H), 0.86 (dd, J = 13.86, 6.91 Hz, 6H).

*((3S,5S,7S)-Adamantan-1-yl)methyl ((S)-1-(((S)-1-Hydroxy-3-((S)-2-oxopyrrolidin-3-yl)propan-2-yl)amino)-4-methyl-1-oxopentan-2-yl)carbamate (**1k**).* Yield (75%). ^{1}H NMR (400 MHz, $CDCl_3$): δ 7.75 (d, J = 7.1 Hz, 1H), 6.15 (s, 1H), 5.27 (d, J = 8.1 Hz, 1H), 4.23−4.18 (m, 1H), 4.03−3.96 (m, 1H), 3.74−3.57 (m, 4H), 3.39−3.31 (m, 2H), 2.49−2.34 (m, 2H), 1.99−1.95 (m, 4H), 1.88−1.79 (m, 1H), 1.76−1.60 (m, 9H), 1.58−1.46 (m, 7H), 0.96 (dd, J = 6.4, 2.4 Hz, 6H).

*((3S,5S,7S)-Adamantan-1-yl)methyl-d_2 ((S)-1-(((S)-1-hydroxy-3-((S)-2-oxopyrrolidin-3-yl)propan-2-yl)amino)-4-methyl-1-oxopentan-2-yl)carbamate (**1l**).* Yield (26%). ^{1}H NMR (400 MHz, cdcl$_3$): δ 7.73 (d, J = 7.3 Hz, 1H), 6.19 (s, 1H), 5.26 (d, J = 8.1 Hz, 1H), 4.22−4.18 (m, 1H), 4.03−3.96 (m, 1H), 3.67−3.54 (m, 2H), 3.39−3.31 (m, 2H), 2.49−2.33 (m, 2H), 2.06−2.02 (m, 1H), 1.99−1.95 (m, 3H), 1.88−1.79 (m, 2H), 1.78−1.60 (m, 9H), 1.57−1.48 (m, 6H), 0.96 (dd, J = 6.4, 2.1 Hz, 6H).

*2-((3S,5S,7S)-Adamantan-1-yl)ethyl ((S)-1-(((S)-1-Hydroxy-3-((S)-2-oxopyrrolidin-3-yl)propan-2-yl)amino)-4-methyl-1-oxopentan-2-yl)carbamate (**1m**).* Yield (65%). ^{1}H NMR (400 MHz, $CDCl_3$): δ 7.73 (d, J = 7.0 Hz, 1H), 6.24 (s, 1H), 5.28 (d, J = 8.3 Hz, 1H), 4.25−4.20 (m, 1H), 4.17−4.07 (m, 2H), 4.04−3.96 (m, 1H), 3.70−3.44 (m, 2H), 3.39−3.31 (m, 2H), 2.52−2.34 (m, 2H), 2.09−1.97 (m, 1H), 1.97−1.91 (m, 3H), 1.90−1.76 (m, 1H), 1.74−1.57 (m, 9H), 1.55−1.45 (m, 7H), 1.40 (t, J = 7.5 Hz, 2H), 0.95 (d, J = 6.4 Hz, 6H).

*((1R,3R,5R,7S)-3-Hydroxyadamantan-1-yl)methyl ((S)-1-(((S)-1-Hydroxy-3-((S)-2-oxopyrrolidin-3-yl)propan-2-yl)amino)-4-methyl-1-oxopentan-2-yl)carbamate (**1n**).* Yield (8%). ^{1}H NMR (400 MHz, $CDCl_3$): δ 7.69 (d, J = 7.3 Hz, 1H), 6.34 (s, 1H), 5.45 (d, J = 8.0 Hz, 1H), 4.20−4.16 (m, 1H), 4.05−3.87 (m, 1H), 3.74−3.54 (m, 4H), 3.37−3.28 (m, 2H), 2.45−2.40 (m, 2H), 2.21 (s, 2H), 2.11−1.94 (m, 1H), 1.88−1.79 (m, 1H), 1.79−1.59 (m, 8H), 1.59−1.54 (m, 2H), 1.54−1.47 (m, 3H), 1.47−1.32 (m, 3H), 0.99−0.88 (m, 6H).

*((1r,3R,5R,7S)-3-Hydroxyadamantan-1-yl)methyl-d_2 ((S)-1-(((S)-1-hydroxy-3-((S)-2-oxopyrrolidin-3-yl)propan-2-yl)amino)-4-methyl-1-oxopentan-2-yl)carbamate (**1o**).* Yield (7%). ^{1}H NMR (400 MHz, $CDCl_3$): δ 7.70 (d, J = 7.1 Hz, 1H), 6.26 (s, 1H), 5.41 (d, J = 7.9 Hz, 1H), 4.23−4.14 (m, 1H), 4.03−3.96 (m, 1H), 3.68−3.54 (m, 2H), 3.39−3.32 (m, 2H), 2.43 (s, 2H), 2.27−2.19 (m, 2H), 2.11−1.91 (m, 1H),

https://doi.org/10.1021/acs.jmedchem.1c00319
J. Med. Chem. XXXX, XXX, XXX−XXX

1.88−1.80 (m, 1H), 1.77−1.60 (m, 8H), 1.60−1.54 (m, 1H), 1.54−1.47 (m, 4H), 1.43−1.38 (m, 3H), 0.99−0.88 (m, 6H).

PREPARATION OF COMPOUNDS 2(A−O)

General Procedure. To a solution of dipeptidyl alcohol **1** (1 equiv) in anhydrous dichloromethane (300 mL/g dipeptidyl alcohol) kept at 0−5 °C under a N_2 atmosphere was added the DMP reagent (3.0 equiv), and the reaction mixture was stirred for 3 h at 15−20 °C. The organic phase was washed with 10% aq $Na_2S_2O_3$ (2 × 100 mL/g dipeptidyl alcohol), followed by saturated aqueous $NaHCO_3$ (2 × 100 mL/g dipeptidyl alcohol), distilled water (2 × 100 mL/g dipeptidyl alcohol), and brine (100 mL/g dipeptidyl alcohol). The organic phase was dried over anhydrous Na_2SO_4, filtered, and concentrated *in vacuo*. The resulting crude product was purified by flash chromatography (hexane/ethyl acetate) to yield aldehyde **2** as a white solid.

*((1R,3s,5S)-Bicyclo[3.3.1]nonan-3-yl)methyl ((S)-4-Methyl-1-oxo-1-(((S)-1-oxo-3-((S)-2-oxopyrrolidin-3-yl)propan-2-yl)-amino)pentan-2-yl)carbamate (**2a**).* Yield (86%). ^{1}H NMR (400 MHz, $CDCl_3$): δ 9.50 (s, 1H), 8.31 (s, 1H), 5.21 (d, J = 8.7 Hz, 1H), 4.38−4.28 (m, 2H), 3.96−3.87 (m, 2H), 3.40−3.31 (m, 2H), 2.54−2.36 (m, 2H), 2.08−1.99 (m, 3H), 1.99−1.81 (m, 5H), 1.76−1.63 (m, 6H), 1.60−1.49 (m, 1H), 1.46−1.29 (m, 4H), 1.15−1.05 (m, 1H), 0.97 (d, J = 6.3 Hz, 6H), 0.88 (d, J = 13.4 Hz, 2H). HRMS m/z: $[M + H]^+$ calcd for $C_{24}H_{40}N_3O_5$, 450.2968; found, 450.2958, m/z: $[M + Na]^+$ calcd for $C_{24}H_{39}N_3NaO_5$, 472.2788; found, 472.2776.

*((1R,3s,5S)-Bicyclo[3.3.1]nonan-3-yl)methyl-d_2 ((S)-4-Methyl-1-oxo-1-(((S)-1-oxo-3-((S)-2-oxopyrrolidin-3-yl)-propan-2-yl)amino)pentan-2-yl)carbamate (**2b**).* Yield (85%). ^{1}H NMR (400 MHz, $CDCl_3$): δ 9.50 (s, 1H), 8.30 (s, 1H), 6.16 (s, 1H), 5.24 (d, J = 8.6 Hz, 1H), 4.38−4.29 (m, 2H), 3.41−3.30 (m, 2H), 2.52−2.34 (m, 2H), 2.12−1.99 (m, 3H), 1.98−1.78 (m, 4H), 1.78−1.62 (m, 4H), 1.61−1.51 (m, 1H), 1.41−1.30 (m, 6H), 1.13−1.06 (m, 1H), 0.97 (d, J = 6.3 Hz, 6H), 0.96−0.83 (m, 2H). HRMS m/z: $[M + Na]^+$ calcd for $C_{24}H_{37}D_2N_3NaO_5$, 474.2913; found, 474.2897.

*((1S,5R)-Bicyclo[3.3.1]non-6-en-3-yl)methyl ((S)-4-Methyl-1-oxo-1-(((S)-1-oxo-3-((S)-2-oxopyrrolidin-3-yl)propan-2-yl)-amino)pentan-2-yl)carbamate (**2c**).* Yield (53%). ^{1}H NMR (400 MHz, $CDCl_3$): δ 9.49 (s, 1H), 8.27 (s, 1H), 6.04 (s, 1H), 5.86 (t, J = 7.1 Hz, 1H), 5.63−5.55 (m, 1H), 5.18 (d, J = 8.5 Hz, 1H), 4.38−4.27 (m, 2H), 4.10−4.03 (m, 1H), 4.03−3.94 (m, 1H), 3.41−3.31 (m, 2H), 2.52−2.37 (m, 1H), 2.28 (s, 2H), 2.18−2.08 (m, 1H), 2.01−1.92 (m, 3H), 1.92−1.83 (m, 3H), 1.83−1.71 (m, 1H), 1.71−1.66 (m, 4H), 1.62−1.49 (m, 3H), 1.49−1.36 (m, 1H), 0.97 (d, J = 6.4 Hz, 6H). HRMS m/z: $[M + H]^+$ calcd for $C_{24}H_{38}N_3O_5$, 448.2811; found, 448.2810, m/z: $[M + Na]^+$ calcd for $C_{24}H_{37}N_3NaO_5$, 470.2631; found, 470.2628.

*((1S,3S,5R)-Bicyclo[3.3.1]non-6-en-3-yl)methyl-d_2 ((S)-4-methyl-1-oxo-1-(((S)-1-oxo-3-((S)-2-oxopyrrolidin-3-yl)-propan-2-yl)amino)pentan-2-yl)carbamate (**2d**).* Yield (88%). ^{1}H NMR (400 MHz, $CDCl_3$): δ 9.49 (s, 1H), 8.28 (d, J = 6.1 Hz, 1H), 6.33 (s, 1H), 5.85 (t, J = 8.0 Hz, 1H), 5.58 (d, J = 9.9 Hz, 1H), 5.24 (d, J = 8.7 Hz, 1H), 4.38−4.29 (m, 2H), 3.43−3.30 (m, 2H), 2.54−2.32 (m, 2H), 2.31−2.26 (m, 1H), 2.20−2.08 (m, 1H), 2.08−1.62 (m, 9H), 1.62−1.46 (m, 4H), 1.45−1.38 (m, 2H), 0.97 (d, J = 6.1 Hz, 6H). HRMS m/z: $[M + Na]^+$ calcd for $C_{24}H_{35}D_2N_3NaO_5$, 472.2757; found, 472.2743.

*Bicyclo[2.2.1]hept-5-en-2-ylmethyl ((S)-4-Methyl-1-oxo-1-(((S)-1-oxo-3-((S)-2-oxopyrrolidin-3-yl)propan-2-yl)amino)-pentan-2-yl)carbamate (**2e**).* Yield (84%). ^{1}H NMR (400 MHz, $CDCl_3$): δ 9.50 (s, 1H), 8.30 (d, J = 6.7 Hz, 1H), 6.39 (s, 1H), 6.14 (dd, J = 5.8, 3.1 Hz, 1H), 5.93 (dd, J = 5.7, 2.9 Hz, 1H), 5.27 (s, 1H), 4.38−4.31 (m, 2H), 3.89−3.80 (m, 1H), 3.69−3.60 (m, 1H), 3.43−3.30 (m, 2H), 2.89−2.78 (m, 1H), 2.56−2.31 (m, 3H), 2.11−1.96 (m, 1H), 1.96−1.90 (m, 1H), 1.90−1.78 (m, 2H), 1.78−1.63 (m, 2H), 1.63−1.49 (m, 1H), 1.48−1.33 (m, 1H), 1.29−1.18 (m, 1H), 1.19−1.10 (m, 1H), 0.97 (d, J = 6.3 Hz, 6H), 0.58−0.50 (m, 1H). HRMS m/z: $[M + Na]^+$ calcd for $C_{22}H_{33}N_3NaO_5$, 442.2318; found, 442.2310.

*Bicyclo[2.2.1]heptan-2-ylmethyl ((S)-4-Methyl-1-oxo-1-(((S)-1-oxo-3-((S)-2-oxopyrrolidin-3-yl)propan-2-yl)amino)-pentan-2-yl)carbamate (**2f**).* Yield (88%). ^{1}H NMR (400 MHz, $CDCl_3$): δ 9.50 (s, 1H), 8.29 (s, 1H), 6.34 (s, 1H), 5.26 (s, 1H), 4.39−4.29 (m, 2H), 4.14−4.03 (m, 1H), 3.97−3.86 (m, 1H), 3.84−3.72 (m, 1H), 3.43−3.30 (m, 2H), 2.54−2.34 (m, 2H), 2.29−2.15 (m, 2H), 2.16−2.08 (m, 1H), 2.08−1.77 (m, 1H), 1.77−1.63 (m, 3H), 1.59−1.43 (m, 2H), 1.41−1.23 (m, 4H), 1.22−1.02 (m, 2H), 0.97 (d, J = 6.3 Hz, 6H), 0.67 (ddd, J = 12.5, 5.4, 2.3 Hz, 1H). HRMS m/z: $[M + Na]^+$ calcd for $C_{22}H_{35}N_3NaO_5$, 444.2475; found, 444.2467.

*tert-Butyl (1R,3s,5S)-3-((((S)-4-methyl-1-oxo-1-(((S)-1-oxo-3-((S)-2-oxopyrrolidin-3-yl)propan-2-yl)amino)pentan-2-yl)-carbamoyl)oxy)-8-azabicyclo[3.2.1]octane-8-carboxylate (**2g**).* Yield (90%). ^{1}H NMR (400 MHz, $CDCl_3$): δ 9.49 (s, 1H), 8.43 (d, J = 5.6 Hz, 1H), 6.07 (s, 1H), 5.20 (d, J = 8.6 Hz, 1H), 4.96 (s, 1H), 4.35−4.28 (m, 2H), 4.25−4.09 (m, 2H), 3.41−3.33 (m, 2H), 2.53−2.36 (m, 2H), 2.23−1.94 (m, 8H), 1.94−1.82 (m, 1H), 1.81−1.64 (m, 4H), 1.61−1.52 (m, 1H), 1.46 (s, 9H), 0.98 (d, J = 5.0 Hz, 6H). HRMS m/z: $[M + H]^+$ calcd for $C_{26}H_{43}N_4O_7$, 523.3131; found, 523.3116. HRMS m/z: $[M + Na]^+$ calcd for $C_{26}H_{42}N_4NaO_7$, 545.2951; found, 545.2938.

*Benzyl (1R,3s,5S)-3-((((S)-4-methyl-1-oxo-1-(((S)-1-oxo-3-((S)-2-oxopyrrolidin-3-yl)propan-2-yl)amino)pentan-2-yl)-carbamoyl)oxy)-8-azabicyclo[3.2.1]octane-8-carboxylate (**2h**).* Yield (66%). ^{1}H NMR (400 MHz, DMSO-d_6): δ 9.39 (s, 1H), 8.55−8.35 (m, 1H), 8.11−8.02 (m, 1H), 7.64 (s, 1H), 7.45−7.19 (m, 5H), 5.75 (s, 1H), 5.09 (d, J = 10.47 Hz, 2H), 4.83−4.71 (m, 2H), 4.21 (s, 2H), 3.73−3.57 (m, 2H), 3.24−3.00 (m, 2H), 2.34−1.79 (m, 3H), 1.79−1.34 (m, 2H), 1.28−1.12 (m, 9H), 0.98−0.77 (m, 6H). HRMS m/z: $[M + H]^+$ calcd for $C_{29}H_{41}N_4O_7$, 557.2970; found, 557.2962. HRMS m/z: $[M + Na]^+$ calcd for $C_{29}H_{40}N_4NaO_7$, 579.2789; found, 579.2773.

*(4-Pentylbicyclo[2.2.2]octan-1-yl)methyl ((S)-4-Methyl-1-oxo-1-(((S)-1-oxo-3-((S)-2-oxopyrrolidin-3-yl)propan-2-yl)-amino)pentan-2-yl)carbamate (**2i**).* Yield (59%). ^{1}H NMR (400 MHz, DMSO-d_6): δ 9.49 (s, 1H), 7.66−7.58 (m, 1H), 7.54−7.44 (m, 2H), 5.72−5.64 (m, 2H), 3.71−3.53 (m, 5H), 3.21−3.13 (m, 1H), 2.93−2.85 (m, 1H), 2.77−2.69 (m, 1H), 2.30−2.22 (m, 1H), 1.91 (s, 1H), 1.63−1.55 (m, 5H), 1.42−0.96 (m, 20H), 0.87 (td, J = 19.27, 6.96, 6.96 Hz, 6H). HRMS m/z: $[M + Na]^+$ calcd for $C_{28}H_{47}N_3NaO_5$, 528.3414; found, 528.3391.

*(4-Pentylbicyclo[2.2.2]octan-1-yl)methyl-d_2 ((S)-4-Methyl-1-oxo-1-(((S)-1-oxo-3-((S)-2-oxopyrrolidin-3-yl)propan-2-yl)-amino)pentan-2-yl)carbamate (**2j**).* Yield (49%). ^{1}H NMR (400 MHz, DMSO-d_6): δ 9.49 (s, 1H), 7.66−7.58 (m, 1H), 7.54−7.44 (m, 2H), 5.72−5.64 (m, 2H), 3.71−3.63 (m, 3H),

https://doi.org/10.1021/acs.jmedchem.1c00319
J. Med. Chem. XXXX, XXX, XXX−XXX

3.31 (s, 1H), 2.93−2.85 (m, 1H), 2.85−2.69 (m, 1H), 2.30−2.22 (m, 1H), 1.91 (s, 1H), 1.42−0.96 (m, 25H), 0.87 (td, J = 19.21, 6.96, 6.96 Hz, 6H). HRMS m/z: $[M + Na]^+$ calcd for $C_{28}H_{45}D_2N_3NaO_5$, 530.3539; found, 530.3536.

*((3S,5S,7S)-Adamantan-1-yl)methyl((S)-4-methyl-1-oxo-1-(((S)-1-oxo-3-((S)-2-oxopyrrolidin-3-yl)propan-2-yl)amino)pentan-2-yl)carbamate (**2k**).* Yield (90%). ^{1}H NMR (400 MHz, $CDCl_3$): δ 9.50 (s, 1H), 8.31 (d, J = 5.8 Hz, 1H), 6.36 (s, 1H), 5.27 (s, 1H), 4.39−4.29 (m, 2H), 3.66 (s, 2H), 3.41−3.30 (m, 2H), 2.55−2.34 (m, 2H), 2.08−1.92 (m, 3H), 1.92−1.78 (m, 2H), 1.78−1.60 (m, 9H), 1.52 (d, J = 2.9 Hz, 7H), 1.00−0.94 (m, 6H). HRMS m/z: $[M + Na]^+$ calcd for $C_{25}H_{39}N_3NaO_5$, 484.2788; found, 484.2780.

*((3S,5S,7S)-Adamantan-1-yl)methyl-d_2 ((S)-4-methyl-1-oxo-1-(((S)-1-oxo-3-((S)-2-oxopyrrolidin-3-yl)propan-2-yl)amino)pentan-2-yl)carbamate (**2l**).* Yield (88%). ^{1}H NMR (400 MHz, cdcl$_3$): δ 9.49 (s, 1H), 8.32 (d, J = 5.9 Hz, 1H), 6.13 (d, J = 8.1 Hz, 1H), 5.23 (s, 1H), 4.68−4.58 (m, 1H), 4.38−4.25 (m, 1H), 3.41−3.27 (m, 2H), 2.52−2.34 (m, 2H), 2.06−2.01 (m, 2H), 2.00−1.89 (m, 3H), 1.88−1.78 (m, 4H), 1.78−1.55 (m, 9H), 1.52 (d, J = 2.9 Hz, 3H), 1.00−0.91 (m, 6H). HRMS m/z: $[M + Na]^+$ calcd for $C_{25}H_{37}D_2N_3NaO_5$, 486.2913; found, 486.2910.

*2-((3S,5S,7S)-Adamantan-1-yl)ethyl ((S)-4-Methyl-1-oxo-1-(((S)-1-oxo-3-((S)-2-oxopyrrolidin-3-yl)propan-2-yl)amino)pentan-2-yl)carbamate (**2m**).* Yield (83%). ^{1}H NMR (400 MHz, $CDCl_3$): δ 9.50 (s, 1H), 8.30 (d, J = 5.9 Hz, 1H), 6.09 (d, J = 11.7 Hz, 1H), 5.19 (d, J = 8.7 Hz, 1H), 4.38−4.28 (m, 2H), 4.26−4.05 (m, 2H), 3.41−3.33 (m, 2H), 2.54−2.35 (m, 2H), 2.01−1.91 (m, 4H), 1.91−1.79 (m, 1H), 1.74−1.58 (m, 9H), 1.51 (d, J = 2.9 Hz, 6H), 1.41 (t, J = 7.4 Hz, 2H), 1.28−1.23 (m, 1H), 0.97 (d, J = 6.4 Hz, 6H). HRMS m/z: $[M + H]^+$ calcd for $C_{26}H_{42}N_3O_5$, 476.3124; found, 476.3124. HRMS m/z: $[M + Na]^+$ calcd for $C_{26}H_{41}N_3NaO_5$, 498.2944; found, 498.2938.

*((1r,3R,5R,7S)-3-Hydroxyadamantan-1-yl)methyl ((S)-4-Methyl-1-oxo-1-(((S)-1-oxo-3-((S)-2-oxopyrrolidin-3-yl)propan-2-yl)amino)pentan-2-yl)carbamate (**2n**).* Yield (47%). ^{1}H NMR (400 MHz, $CDCl_3$): δ 9.49 (s, 1H), 8.28 (d, J = 23.9 Hz, 1H), 6.19 (s, 1H), 5.19 (s, 1H), 4.34−4.03 (m, 2H), 4.02−3.61 (m, 2H), 2.89−2.58 (m, 2H), 2.58−2.28 (m, 2H), 2.28−2.13 (m, 3H), 2.09−1.76 (m, 2H), 1.78−1.60 (m, 6H), 1.57−1.31 (m, 9H), 1.01−0.91 (m, 6H). HRMS m/z: $[M + Na]^+$ calcd for $C_{25}H_{39}N_3NaO_6$, 500.2737; found, 500.2739.

*((1r,3R,5R,7S)-3-Hydroxyadamantan-1-yl)methyl-d_2 ((S)-4-Methyl-1-oxo-1-(((S)-1-oxo-3-((S)-2-oxopyrrolidin-3-yl)propan-2-yl)amino)pentan-2-yl)carbamate (**2o**).* Yield (44%). ^{1}H NMR (400 MHz, $CDCl_3$): δ 9.48 (s, 1H), 8.28 (d, J = 6.5 Hz, 1H), 6.39 (s, 1H), 5.12 (s, 1H), 4.40−4.09 (m, 2H), 2.89−2.59 (m, 2H), 2.56−2.30 (m, 2H), 2.30−2.20 (m, 3H), 2.18−1.77 (m, 2H), 1.77−1.61 (m, 6H), 1.59−1.39 (m, 9H), 1.01−0.89 (m, 6H). HRMS m/z: $[M + Na]^+$ calcd for $C_{25}H_{37}D_2N_3NaO_6$, 502.2862; found, 502.2860.

PREPARATION OF COMPOUNDS 3(A−O)

General Procedure. To a solution of dipeptidyl aldehyde **2** (1 equiv) in ethyl acetate (10 mL/g dipeptidyl aldehyde) was added absolute ethanol (5 mL/g dipeptidyl aldehyde) with stirring, followed by a solution of sodium bisulfite (1 equiv) in water (1 mL/g dipeptidyl aldehyde). The reaction mixture was stirred for 3 h at 50 °C. The reaction mixture was allowed to cool to room temperature and then vacuum-filtered. The solid was thoroughly washed with absolute ethanol, and the filtrate was dried over anhydrous sodium sulfate, filtered, and concentrated to yield a white solid. The white solid was stirred with dry ethyl ether (3 × 10 mL/g dipeptidyl aldehyde), followed by careful removal of the solvent using a pipette and dried using a vacuum pump for 2 h to yield dipeptidyl bisulfite adduct **3** as a white solid.

*Sodium (2S)-2-((2S)-2-((((((1R,5S)-Bicyclo[3.3.1]nonan-3-yl)methoxy)carbonyl)amino)-4-methylpentanamido)-1-hydroxy-3-((S)-2-oxopyrrolidin-3-yl)propane-1-sulfonate (**3a**).* Yield (66%). ^{1}H NMR (400 MHz, DMSO-d_6): δ 7.61 (d, J = 9.0 Hz, 1H), 7.57−7.44 (m, 1H), 7.28−7.08 (m, 1H), 5.62 (d, J = 6.1 Hz, 1H), 5.47 (d, J = 5.9 Hz, 1H), 4.12−3.91 (m, 2H), 3.91−3.73 (m, 2H), 3.16−3.00 (m, 2H), 2.24−2.07 (m, 2H), 2.06−1.95 (m, 2H), 1.83 (dt, J = 17.2, 7.2 Hz, 4H), 1.74−1.51 (m, 5H), 1.51−1.38 (m, 2H), 1.35−1.15 (m, 6H), 1.14−1.00 (m, 2H), 0.99−0.81 (m, 6H). HRMS m/z: $[M + Na]^+$ calcd for $C_{24}H_{40}N_3Na_2O_8S$, 576.2332; found, 576.2329, m/z: $[M]^-$ calcd for $C_{24}H_{40}N_3O_8S$, 530.2536; found, 530.2529.

*Sodium (2S)-2-((S)-2-(((((1R,3s,5S)-Bicyclo[3.3.1]nonan-3-yl)methoxy-d_2)carbonyl)amino)-4-methylpentanamido)-1-hydroxy-3-((S)-2-oxopyrrolidin-3-yl)propane-1-sulfonate (**3b**).* Yield (75%). ^{1}H NMR (400 MHz, DMSO-d_6): δ 7.63−7.43 (m, 2H), 7.20 (dd, J = 20.3, 8.2 Hz, 1H), 5.52−5.33 (m, 1H), 4.06−3.78 (m, 2H), 3.20−2.99 (m, 2H), 2.33−2.04 (m, 3H), 2.04−1.93 (m, 2H), 1.94−1.74 (m, 2H), 1.74−1.50 (m, 3H), 1.50−1.38 (m, 2H), 1.38−1.19 (m, 5H), 1.11−0.98 (m, 2H), 0.97−0.80 (m, 10H). HRMS m/z: $[M + Na]^+$ calcd for $C_{24}H_{38}D_2N_3Na_2O_8S$, 578.2457; found, 578.2432.

*Sodium (2S)-2-((2S)-2-((((((1S,5R)-Bicyclo[3.3.1]non-6-en-3-yl)methoxy)carbonyl)amino)-4-methylpentanamido)-1-hydroxy-3-((S)-2-oxopyrrolidin-3-yl)propane-1-sulfonate (**3c**).* Yield (66%). ^{1}H NMR (400 MHz, DMSO-d_6): δ 7.52 (d, J = 9.5 Hz, 1H), 7.47 (d, J = 4.5 Hz, 1H), 7.18 (ddd, J = 19.5, 8.5, 2.7 Hz, 1H), 5.89−5.79 (m, 1H), 5.58−5.52 (m, 1H), 3.97 (h, J = 8.1 Hz, 1H), 3.90−3.70 (m, 1H), 3.27−3.00 (m, 2H), 2.35−2.19 (m, 3H), 2.19−2.02 (m, 3H), 2.02−1.68 (m, 6H), 1.68−1.49 (m, 4H), 1.49−1.25 (m, 6H), 1.13−1.04 (m, 1H), 0.91−0.79 (m, 6H). HRMS m/z: $[M + Na]^+$ calcd for $C_{24}H_{38}N_3Na_2O_8S$, 574.2175; found, 574.2163, m/z: $[M]^-$ calcd for $C_{24}H_{38}N_3O_8S$, 528.2379; found, 528.2367.

*Sodium (2S)-2-((S)-2-(((((1S,3S,5R)-Bicyclo[3.3.1]non-6-en-3-yl)methoxy-d_2)carbonyl)amino)-4-methylpentanamido)-1-hydroxy-3-((S)-2-oxopyrrolidin-3-yl)propane-1-sulfonate (**3d**).* Yield (53%). ^{1}H NMR (400 MHz, DMSO-d_6): δ 7.62−7.39 (m, 2H), 7.18 (dd, J = 24.9, 8.5 Hz, 1H), 5.89−5.80 (m, 1H), 5.59−5.52 (m, 1H), 5.43−5.26 (m, 1H), 4.06−3.67 (m, 2H), 3.22−2.98 (m, 2H), 2.37−2.03 (m, 5H), 2.03−1.64 (m, 5H), 1.64−1.52 (m, 3H), 1.52−1.29 (m, 5H), 1.13−1.02 (m, 1H), 0.89−0.80 (m, 6H). HRMS m/z: $[M + Na]^+$ calcd for $C_{24}H_{36}D_2N_3Na_2O_8S$, 576.2301; found, 576.2275.

*Sodium (2S)-2-((2S)-2-(((Bicyclo[2.2.1]hept-5-en-2-ylmethoxy)carbonyl)amino)-4-methylpentanamido)-1-hydroxy-3-((S)-2-oxopyrrolidin-3-yl)propane-1-sulfonate (**3e**).* Yield (56%). ^{1}H NMR (400 MHz, DMSO-d_6): δ 7.68−7.37 (m, 2H), 7.32−7.17 (m, 1H), 6.20−6.02 (m, 1H), 6.02−5.86 (m, 1H), 5.59−5.30 (m, 1H), 4.11−3.79 (m, 2H), 3.79−3.41 (m, 2H), 3.21−2.98 (m, 2H), 2.87−2.66 (m, 2H), 2.39−2.04 (m, 3H), 2.04−1.85 (m, 1H), 1.85−1.70 (m, 1H), 1.70−1.51 (m, 2H), 1.50−1.36 (m, 2H), 1.28 (dd, J = 39.4, 7.9 Hz, 2H), 1.18−1.00 (m, 1H), 0.93−0.79 (m, 6H), 0.47 (d, J = 11.6 Hz,

https://doi.org/10.1021/acs.jmedchem.1c00319
J. Med. Chem. XXXX, XXX, XXX−XXX

1H). HRMS m/z: $[M + Na]^+$ calcd for $C_{22}H_{34}N_3Na_2O_8S$, 546.1862; found, 546.1842.

Sodium (2S)-2-((2S)-2-(((Bicyclo[2.2.1]heptan-2-ylmethoxy)carbonyl)amino)-4-methylpentanamido)-1-hydroxy-3-((S)-2-oxopyrrolidin-3-yl)propane-1-sulfonate (**3f**). Yield (66%). ^{1}H NMR (400 MHz, DMSO-d_6): δ 7.61−7.39 (m, 2H), 7.32−7.08 (m, 1H), 5.41 (dd, J = 55.1, 5.9 Hz, 1H), 4.07−3.55 (m, 2H), 3.18−2.99 (m, 2H), 2.28−2.04 (m, 6H), 2.04−1.81 (m, 1H), 1.81−1.53 (m, 3H), 1.53−1.36 (m, 5H), 1.36−1.18 (m, 3H), 1.18−0.91 (m, 2H), 0.90−0.75 (m, 6H), 0.70−0.59 (m, 1H). HRMS m/z: $[M + Na]^+$ calcd for $C_{22}H_{36}N_3Na_2O_8S$, 548.2019; found, 548.1999.

Sodium (2S)-2-((S)-2-(((((1R,3s,5S)-8-(tert-Butoxycarbonyl)-8-azabicyclo[3.2.1]octan-3-yl)oxy)carbonyl)amino)-4-methylpentanamido)-1-hydroxy-3-((S)-2-oxopyrrolidin-3-yl)propane-1-sulfonate (**3g**). Yield (52%). ^{1}H NMR (400 MHz, DMSO-d_6): δ 7.64−7.51 (m, 1H), 7.46 (d, J = 3.8 Hz, 1H), 7.30 (dd, J = 19.2, 8.3 Hz, 1H), 5.55−5.31 (m, 1H), 4.76 (s, 1H), 4.02−3.78 (m, 4H), 3.22−2.98 (m, 2H), 2.27−1.68 (m, 9H), 1.66−1.57 (m, 4H), 1.51−1.43 (m, 2H), 1.40 (s, 9H), 1.13−1.02 (m, 1H), 0.91−0.81 (m, 6H). HRMS m/z: $[M + Na]^+$ calcd for $C_{26}H_{43}N_4Na_2O_{10}S$, 649.2496; found, 649.2500.

Sodium (2S)-2-((S)-2-(((((1R,3s,5S)-8-((Benzyloxy)carbonyl)-8-azabicyclo[3.2.1]octan-3-yl)oxy)carbonyl)amino)-4-methylpentanamido)-1-hydroxy-3-((S)-2-oxopyrrolidin-3-yl)propane-1-sulfonate (**3h**). Yield (53%). ^{1}H NMR (400 MHz, DMSO-d_6): δ 7.37 (t, J = 4.74, 4.74 Hz, 8H), 5.09 (d, J = 11.06 Hz, 2H), 4.29−4.13 (m, 5H), 3.96−3.82 (m, 1H), 3.79−3.69 (m, 1H), 3.17−3.09 (m, 1H), 3.06−2.98 (m, 1H), 2.05−1.81 (m, 5H), 1.74−1.63 (m, 3H), 1.58−1.49 (m, 4H), 1.47−1.33 (m, 2H), 1.08 (dd, J = 13.72, 6.78 Hz, 1H), 0.84 (ddd, J = 10.35, 8.11, 4.59 Hz, 6H). HRMS m/z: $[M + Na]^+$ calcd for $C_{29}H_{41}N_4Na_2O_{10}S$, 683.2339; found, 683.2317.

Sodium (2S)-1-Hydroxy-2-((S)-4-methyl-2-((((4-pentylbicyclo[2.2.2]octan-1-yl)methoxy)carbonyl)amino)-pentanamido)-3-((S)-2-oxopyrrolidin-3-yl)propane-1-sulfonate (**3i**). Yield (57%). ^{1}H NMR (400 MHz, DMSO-d_6): δ 7.51−7.40 (m, 3H), 4.00−3.53 (m, 5H), 3.49−3.40 (m, 1H), 3.16−2.98 (m, 4H), 1.94−1.85 (m, 3H), 1.65−0.96 (m, 25H), 0.85 (dd, J = 12.73, 5.76 Hz, 6H). HRMS m/z: $[M + Na]^+$ calcd for $C_{28}H_{48}N_3Na_2O_8S$, 632.2958; found, 632.2932. HRMS m/z: $[M]^-$ calcd for $C_{28}H_{48}N_3O_8S$, 586.3168; found, 586.3163.

Sodium (2S)-1-Hydroxy-2-((S)-4-methyl-2-((((4-pentylbicyclo[2.2.2]octan-1-yl)methoxy-d_2)carbonyl)-amino)pentanamido)-3-((S)-2-oxopyrrolidin-3-yl)propane-1-sulfonate (**3j**). Yield (50%). ^{1}H NMR (400 MHz, DMSO-d_6): δ 7.51−7.40 (m, 3H), 4.00−3.53 (m, 3H), 3.40−3.26 (m, 1H), 3.16−2.90 (m, 3H), 2.56−2.44 (m, 1H), 1.95−1.85 (m, 3H), 1.65−0.96 (m, 25H), 0.85 (dd, J = 12.73, 5.76 Hz, 6H). HRMS m/z: $[M + Na]^+$ calcd for $C_{28}H_{46}D_2N_3Na_2O_8S$, 634.3083; found, 634.3071. HRMS m/z: $[M]^-$ calcd for $C_{28}H_{46}D_2N_3O_8S$, 588.3287; found, 588.3399.

Sodium (2S)-2-((S)-2-(((((3S,5S,7S)-Adamantan-1-yl)-methoxy)carbonyl)amino)-4-methylpentanamido)-1-hydroxy-3-((S)-2-oxopyrrolidin-3-yl)propane-1-sulfonate (**3k**). Yield (52%). ^{1}H NMR (400 MHz, DMSO-d_6): δ 7.66−7.41 (m, 2H), 7.25−7.10 (m, 1H), 5.40 (dd, J = 47.1, 6.0 Hz, 1H), 4.10−3.70 (m, 2H), 3.69−3.47 (m, 2H), 3.18−3.00 (m, 2H), 2.24−2.03 (m, 2H), 2.03−1.83 (m, 4H), 1.83−1.55 (m, 8H), 1.55−1.33 (m, 6H), 1.13−1.02 (m, 1H), 0.93−0.80 (m, 6H). HRMS m/z: $[M + Na]^+$ calcd for $C_{25}H_{40}N_3Na_2O_8S$, 588.2332; found, 588.2310.

Sodium (2S)-2-((S)-2-(((((3S,5S,7S)-Adamantan-1-yl)-methoxy-d_2)carbonyl)amino)-4-methylpentanamido)-1-hydroxy-3-((S)-2-oxopyrrolidin-3-yl)propane-1-sulfonate (**3l**). Yield (39%). ^{1}H NMR (400 MHz, DMSO-d_6): δ 7.63−7.50 (m, 1H), 7.47−7.36 (m, 1H), 7.38−7.28 (m, 1H), 5.41 (dd, J = 36.5, 6.0 Hz, 1H), 4.27−4.19 (m, 1H), 3.99−3.94 (m, 1H), 3.49−3.34 (m, 1H), 3.21−3.01 (m, 2H), 2.25−1.99 (m, 2H), 1.99−1.90 (m, 3H), 1.89−1.73 (m, 3H), 1.72−1.52 (m, 9H), 1.48 (s, 5H), 0.90−0.76 (m, 6H). HRMS m/z: $[M + Na]^+$ calcd for $C_{25}H_{38}D_2N_3Na_2O_8S$, 590.2457; found, 590.2447.

Sodium (2S)-2-((S)-2-(((2-((3S,5S,7S)-Adamantan-1-yl)-ethoxy)carbonyl)amino)-4-methylpentanamido)-1-hydroxy-3-((S)-2-oxopyrrolidin-3-yl)propane-1-sulfonate (**3m**). Yield (60%). ^{1}H NMR (400 MHz, DMSO-d_6): δ 7.62−7.49 (m, 1H), 7.49−7.43 (m, 1H), 7.24−7.07 (m, 1H), 5.40 (dd, J = 48.6, 6.1 Hz, 1H), 4.05−3.81 (m, 4H), 3.20−3.00 (m, 2H), 2.26−2.06 (m, 2H), 2.01−1.87 (m, 3H), 1.84−1.72 (m, 1H), 1.70−1.54 (m, 10H), 1.49 (d, J = 3.0 Hz, 6H), 1.45−1.38 (m, 1H), 1.38−1.28 (m, 2H), 0.89−0.80 (m, 6H). HRMS m/z: $[M + Na]^+$ calcd for $C_{26}H_{42}N_3Na_2O_8S$, 602.2488; found, 602.2480.

Sodium (2S)-1-Hydroxy-2-((S)-2-(((((1r,3R,5R,7S)-3-hydroxyadamantan-1-yl)methoxy)carbonyl)amino)-4-methylpentanamido)-3-((S)-2-oxopyrrolidin-3-yl)propane-1-sulfonate (**3n**). Yield (69%). ^{1}H NMR (400 MHz, acetone): δ 7.08−7.03 (m, 1H), 7.00−6.95 (m, 1H), 6.45−6.41 (m, 1H), 4.38−3.89 (m, 2H), 3.89−3.53 (m, 2H), 2.96−2.53 (m, 1H), 2.53−2.25 (m, 2H), 2.16 (s, 2H), 1.99−1.70 (m, 4H), 1.70−1.62 (m, 5H), 1.62−1.53 (m, 4H), 1.53−1.35 (m, 5H), 1.34−1.16 (m, 1H), 0.99−0.85 (m, 6H). HRMS m/z: $[M + Na]^+$ calcd for $C_{25}H_{40}N_3Na_2O_9S$, 604.2282; found, 604.2273.

Sodium (2S)-1-Hydroxy-2-((S)-2-(((((1r,3R,5R,7S)-3-hydroxyadamantan-1-yl)methoxy-d_2)carbonyl)amino)-4-methylpentanamido)-3-((S)-2-oxopyrrolidin-3-yl)propane-1-sulfonate (**3o**). Yield (73%). ^{1}H NMR (400 MHz, acetone): δ 7.10−7.05 (m, 1H), 6.91−6.87 (m, 1H), 6.43−6.38 (m, 1H), 4.33−4.06 (m, 2H), 3.33−3.19 (m, 2H), 2.50−2.24 (m, 1H), 2.22−2.10 (m, 3H), 2.03−1.71 (m, 2H), 1.70−1.61 (m, 5H), 1.61−1.52 (m, 5H), 1.52−1.38 (m, 6H), 1.01−0.85 (m, 6H). HRMS m/z: $[M + Na]^+$ calcd for $C_{25}H_{38}D_2N_3Na_2O_9S$, 606.2406; found, 606.2409.

BIOCHEMICAL STUDIES

Enzyme Assays and Inhibition Studies. *Cloning and Expression of the 3CL Protease of SARS-CoV-2 and FRET Enzyme Assays.* The codon-optimized cDNA of full length of 3CLpro of SARS-CoV-2 (GenBank number MN908947.3) fused with sequences encoding six histidines at the N-terminal was synthesized by Integrated DNA (Coralville, IA). The synthesized gene was subcloned into the pET-28a(+) vector. The expression and purification of SARS-CoV-2 3CLpro were conducted following a standard procedure described previously.[17,18,25] Briefly, a stock solution of an inhibitor was prepared in DMSO and diluted in assay buffer composed of 20 mM HEPES buffer, pH 8, containing NaCl (200 mM), EDTA (0.4 mM), glycerol (60%), and 6 mM dithiothreitol. The SARS-CoV-2 protease was mixed with serial dilutions of the inhibitor or with DMSO in 25 μL of assay buffer and incubated at 37 °C for 1 h, followed by the addition of 25 μL of assay buffer containing the substrate (FAM-SAVLQ/SG-QXL520, AnaSpec, Fremont, CA). The substrate was derived from the

https://doi.org/10.1021/acs.jmedchem.1c00319
J. Med. Chem. XXXX, XXX, XXX−XXX

cleavage sites on the viral polyproteins of SARS-CoV. Fluorescence readings were obtained using an excitation wavelength of 480 nm and an emission wavelength of 520 nm on a fluorescence microplate reader (FLx800; Biotec, Winoosk, VT) for 1 h following the addition of the substrate. Relative fluorescence units were determined by subtracting background values (substrate-containing well without protease) from the raw fluorescence values, as described previously.[25] The dose-dependent FRET inhibition curves were fitted with a variable slope using GraphPad Prism software (GraphPad, La Jolla, CA) in order to determine the IC_{50} values of the compounds. The expression and purification of the 3CLpro of MERS-CoV and the FRET enzyme assays were performed as described previously.[17,18,25]

Cell-Based Assay for Antiviral Activity. Compounds **2a** and **3a** were investigated for their antiviral activity against the replication of SARS-CoV-2. Briefly, confluent Vero E6 cells were inoculated with SARS-CoV-2 at 50−100 plaque-forming units/well, and medium containing various concentrations of each compound and agar was applied to the cells. After 48−72 h, plaques in each well were counted. The 50% effective concentration (EC_{50}) values were determined using GraphPad Prism software using a variable slope (GraphPad, La Jolla, CA).

Nonspecific Cytotoxic Effects/*in Vitro* Cytotoxicity. Confluent cells grown in 96-well plates were incubated with various concentrations (1−100 μM) of each compound for 72 h. Cell cytotoxicity was measured using a CytoTox 96 nonradioactive cytotoxicity assay kit (Promega, Madison, WI), and the CC_{50} values were calculated using a variable slope using GraphPad Prism software. The *in vitro* SI was calculated by dividing the CC_{50} by the IC_{50}.

X-RAY CRYSTALLOGRAPHIC STUDIES

Crystallization and Data Collection. Purified SARS-2 3CL protease (SARS-2 3CLpro) in 100 mM NaCl and 20 mM Tris buffer, pH 8.0, was concentrated to 9.6 mg/mL (0.28 mM) for crystallization screening. All crystallization experiments were set up using an NT8 drop-setting robot (Formulatrix Inc.) and UVXPO MRC (Molecular Dimensions) sitting drop vapor diffusion plates at 18 °C. Protein (100 nL) and 100 nL of crystallization solution were dispensed and equilibrated against 50 μL of the latter. Stock solutions of the inhibitors (100 mM) were prepared in DMSO, and the complexes were obtained by mixing 1 μL of the ligand (2 mM) with 49 μL (0.28 mM) of SARS-2 3CLpro and incubating on ice for 1 h. Crystals were obtained in 1−2 days from the following conditions. **2a** and **3b**: Berkeley screen (Rigaku Reagents) condition C5 (20% (w/v) PEG 4000, 100 mM Tris pH 8.0), **2f**: Index HT screen (Hampton Research) condition H6 (20% (w/v) PEG 3350, 200 mM sodium formate), **2k**: Proplex HT screen (Molecular Dimensions) condition D7 (15% (w/v) PEG 6000, 100 mM sodium citrate pH 5.5), **3c** and **3d**: the Berkeley screen (Rigaku Reagents) condition D9 (20% (w/v) PEG 3350, 100 mM Bis-Tris pH 6.5, 100 mM ammonium phosphate dibasic, 5% (v/v) 2-propanol), and **3e:** Index HT screen (Hampton Research) condition C5 (15% (w/v) PEG 3350, 100 mM succinic acid pH 7.0). Samples were transferred to cryoprotectant solutions, prior to plunging in liquid nitrogen, composed of 80% crystallization solution and 20% (v/v) PEG 200 except for **3c** and **3d** for which 20% (v/v) ethylene glycol was used as the cryoprotectant. X-ray diffraction data were collected at the Advanced Photon Source IMCA-CAT beamline 17-ID except for the data for the complex with **3c** which were collected at the National Synchrotron Light Source II (NSLS-II) AMX beamline 17-ID-1.

Structure Solution and Refinement. Intensities were integrated using XDS[30,31] via Autoproc,[32] and the Laue class analysis and data scaling were performed with Aimless.[33] Structure solution was conducted by molecular replacement with Phaser[34] using a previously determined structure of SARS-2 3CLpro (PDB 6XMK) as the search model. Structure refinement and manual model building were conducted with Phenix[35] and Coot,[36] respectively. Disordered side chains were truncated to the point for which electron density could be observed. Structure validation was conducted with MolProbity,[37] and structure analysis/figure preparation were carried out using the CCP4mg package.[38] Crystallographic data are provided in Table S1.[39−43]

ASSOCIATED CONTENT

Supporting Information

The Supporting Information is available free of charge at https://pubs.acs.org/doi/10.1021/acs.jmedchem.1c00319.

Binding mode of the 3b with SARS-CoV-2 3CLpro; Superposition of 3b with 2a, 3c with 3d; Surface representation showing the orientation 2f, 2k and 3e in subunit B near the S4 subsite of SARS-CoV-2 3CLpro; and Crystallographic data for SARS-CoV-2 3CLpro inhibitor complexes (PDF)

Molecular formula strings—SMILES codes (CSV)

Accession Codes

Coordinates and structure factors for the following SARS2 3CLpro complexes with inhibitors were deposited to the Worldwide Protein Databank (wwPDB) with the accession codes 7LKR (**2a**), 7LKS (**2f**), 7LKT (**2k**), 7LKU (**3b**), 7LKV (**3c**), 7LKW (**3d**), and 7LKX (**3e**). Authors will release the atomic coordinates upon article publication.

AUTHOR INFORMATION

Corresponding Authors

Kyeong-Ok Chang − *Department of Diagnostic Medicine & Pathobiology, College of Veterinary Medicine, Kansas State University, Manhattan, Kansas 66506, United States*; Phone: (316) 978 7374; Email: bill.groutas@wichita.edu

William C. Groutas − *Department of Chemistry, Wichita State University, Wichita, Kansas 67260, United States*; orcid.org/0000-0001-5248-7912; Phone: (785) 532 3849; Email: kchang@vet.ksu.edu

Authors

Chamandi S. Dampalla − *Department of Chemistry, Wichita State University, Wichita, Kansas 67260, United States*; orcid.org/0000-0002-8199-2376

Yunjeong Kim − *Department of Diagnostic Medicine & Pathobiology, College of Veterinary Medicine, Kansas State University, Manhattan, Kansas 66506, United States*

Naemi Bickmeier − *Department of Diagnostic Medicine & Pathobiology, College of Veterinary Medicine, Kansas State University, Manhattan, Kansas 66506, United States*

Athri D. Rathnayake − *Department of Chemistry, Wichita State University, Wichita, Kansas 67260, United States*; orcid.org/0000-0003-2588-7624

https://doi.org/10.1021/acs.jmedchem.1c00319
J. Med. Chem. XXXX, XXX, XXX−XXX

Harry Nhat Nguyen − *Department of Chemistry, Wichita State University, Wichita, Kansas 67260, United States*
Jian Zheng − *Department of Microbiology and Immunology, Carver College of Medicine, University of Iowa, Iowa City, Iowa 52242, United States*
Maithri M. Kashipathy − *Protein Structure Laboratory, The University of Kansas, Lawrence, Kansas 66047, United States*
Matthew A. Baird − *Department of Chemistry, Wichita State University, Wichita, Kansas 67260, United States*
Kevin P. Battaile − *NYX, New York Structural Biology Center, Upton, New York 11973, United States;* orcid.org/0000-0003-0833-3259
Scott Lovell − *Protein Structure Laboratory, The University of Kansas, Lawrence, Kansas 66047, United States*
Stanley Perlman − *Department of Microbiology and Immunology, Carver College of Medicine, University of Iowa, Iowa City, Iowa 52242, United States*

Complete contact information is available at: https://pubs.acs.org/10.1021/acs.jmedchem.1c00319

Notes

The authors declare no competing financial interest.

■ ACKNOWLEDGMENTS

This research was supported in part by grants from the National Institutes of Health (NIH) (R01 AI109039 to K.O.C. and P01 AI060699 and R01 AI129269 to S.P.). The use of the University of Kansas Protein Structure Laboratory was supported by a grant from the National Institute of General Medical Sciences (P30GM110761) of the NIH. The use of the IMCA-CAT beamline 17-ID at the Advanced Photon Source was supported by the companies of the Industrial Macromolecular Crystallography Association through a contract with Hauptman-Woodward Medical Research Institute. The use of the Advanced Photon Source was supported by the U.S. Department of Energy, Office of Science, Office of Basic Energy Sciences under contract no. DE-AC02-06CH11357. This research used the AMX beamline of the National Synchrotron Light Source II, a U.S. Department of Energy (DOE) Office of Science User Facility operated for the DOE Office of Science by Brookhaven National Laboratory under Contract no. DE-SC0012704. The Center for BioMolecular Structure (CBMS) is primarily supported by the National Institutes of Health, National Institute of General Medical Sciences (NIGMS) through a Center Core P30 grant (P30GM133893), and the DOE Office of Biological and Environmental Research (KP1605010).

■ ABBREVIATIONS

ORF, open reading frame; DSC, *N,N′*-disuccinimidyl carbonate; TEA, triethyl amine; DMP, Dess-Martin periodinane; DTT, dithiothreitol; DMSO, dimethyl sulfoxide; MNV, murine norovirus; MOI, multiplicity of infection; CPE, cytopathic effects; $TCID_{50}$, the 50% tissue culture infectious dose; IC_{50}, the 50% inhibitory concentration in the enzyme assay; EC_{50}, the 50% effective concentration in cell culture; CC_{50}, 50% cytotoxic concentration in cell-based assays; GESAMT, general efficient structural alignment of macromolecular targets; RMSD, root mean square deviation; XDS, X-ray detector software; MME, monomethyl ether; PK, pharmacokinetics.

■ REFERENCES

(1) Perlman, S., Masters, P. S. Coronaviridae: The Viruses and Their Replication. In *Fields Virology: Emerging Viruses*; Howley, P. M., Knipe, D. M., Whelan, S., Eds.; Wolters Kluwer: Wichita, 2020; Vol. *1*, pp 410−448.
(2) Hu, T.; Liu, Y.; Zhao, M.; Zhuang, Q.; Xu, L.; He, Q. A comparison of COVID-19, SARS and MERS. *PeerJ* **2020**, *8*, No. e9725.
(3) Wu, F.; Zhao, S.; Yu, B.; Chen, Y.-M.; Wang, W.; Song, Z.-G.; Hu, Y.; Tao, Z.-W.; Tian, J.-H.; Pei, Y.-Y.; Yuan, M.-L.; Zhang, Y.-L.; Dai, F.-H.; Liu, Y.; Wang, Q.-M.; Zheng, J.-J.; Xu, L.; Holmes, E. C.; Zhang, Y.-Z. A new coronavirus associated with human respiratory disease in China. *Nature* **2020**, *579*, 265−269.
(4) Dong, E.; Du, H.; Gardner, L. An interactive web-based dashboard to track COVID-19 in real time. *Lancet Infect. Dis.* **2020**, *20*, 533−534.
(5) Ghosh, A. K.; Brindisi, M.; Shahabi, D.; Chapman, M. E.; Mesecar, A. D. Drug Development and Medicinal Chemistry Efforts toward SARS-Coronavirus and Covid-19 Therapeutics. *ChemMedChem* **2020**, *15*, 907−932.
(6) Gil, C.; Ginex, T.; Maestro, I.; Nozal, V.; Barrado-Gil, L.; Cuesta-Geijo, M. Á.; Urquiza, J.; Ramírez, D.; Alonso, C.; Campillo, N. E.; Martinez, A. COVID-19: Drug targets and potential treatments. *J. Med. Chem.* **2020**, *63*, 12359−12386.
(7) Sharma, A.; Tiwari, S.; Deb, M. K.; MARTY, J. L. Severe acute respiratory syndrome coronavirus-2 (SARS-CoV-2): a global pandemic and treatment strategies. *Int. J. Antimicrob. Agents* **2020**, *56*, 106054.
(8) Cannalire, R.; Cerchia, C.; Beccari, A. R.; Di Leva, F. S.; Summa, V. Targeting SARS-CoV-2 proteases and polymerase for COVID-19 treatment: State of the art and future opportunities. *J. Med. Chem.* [Online early access]. DOI: 10.1021/acs.jmedchem.0c01140. Published online: Nov 13, **2020**. https://doi.org/10.1021/acs.jmedchem.0c01140 (accessed Nov 13, 2020).
(9) Ullrich, S.; Nitsche, C. The SARS-CoV-2 main protease as drug target. *Bioorg. Med. Chem. Lett.* **2020**, *30*, 127377.
(10) Rut, W.; Lv, Z.; Zmudzinski, M.; Patchett, S.; Nayak, D.; Snipas, S. J.; El Oualid, F.; Huang, T. T.; Bekes, M.; Drag, M.; Olsen, S. K. Activity profiling and crystal structures of inhibitor-bound SARS-CoV-2 papain-like protease: A framework for anti-COVID-19 drug design. *Sci. Adv.* **2020**, *6*, No. eabd4596.
(11) Jin, Z.; Du, X.; Xu, Y.; Deng, Y.; Liu, M.; Zhao, Y.; Zhang, B.; Li, X.; Zhang, L.; Peng, C.; Duan, Y.; Yu, J.; Wang, L.; Yang, K.; Liu, F.; Jiang, R.; Yang, X.; You, T.; Liu, X.; Yang, X.; Bai, F.; Liu, H.; Liu, X.; Guddat, L. W.; Xu, W.; Xiao, G.; Qin, C.; Shi, Z.; Jiang, H.; Rao, Z.; Yang, H. Structure of Mpro from SARS-CoV-2 and discovery of its inhibitors. *Nature* **2020**, *582*, 289−293.
(12) Zhang, L.; Lin, D.; Sun, X.; Curth, U.; Drosten, C.; Sauerhering, L.; Becker, S.; Rox, K.; Hilgenfeld, R. Crystal structure of SARS-CoV-2 main protease provides a basis for design of improved α-ketoamide inhibitors. *Science* **2020**, *368*, 409−412.
(13) Dai, W.; Zhang, B.; Jiang, X.-M.; Su, H.; Li, J.; Zhao, Y.; Xie, X.; Jin, Z.; Peng, J.; Liu, F.; Li, C.; Li, Y.; Bai, F.; Wang, H.; Cheng, X.; Cen, X.; Hu, S.; Yang, X.; Wang, J.; Liu, X.; Xiao, G.; Jiang, H.; Rao, Z.; Zhang, L.-K.; Xu, Y.; Yang, H.; Liu, H. Structure-based design of antiviral drug candidates targeting the SARS-CoV-2 main protease. *Science* **2020**, *368*, 1331−1335.
(14) Hoffman, R. L.; Kania, R. S.; Brothers, M. A.; Davies, J. F.; Ferre, R. A.; Gajiwala, K. S.; He, M.; Hogan, R. J.; Kozminski, K.; Li, L. Y.; Lockner, J. W.; Lou, J.; Marra, M. T.; Mitchell, L. J., Jr; Murray, B. W.; Nieman, J. A.; Noell, S.; Planken, S. P.; Rowe, T.; Ryan, K.; Smith, G. J., III; Solowiej, J. E.; Steppan, C. M.; Taggart, B. Discovery of ketone-based covalent inhibitors of coronavirus 3CL proteases for the potential therapeutic treatment of COVID-19. *J. Med. Chem.* **2020**, *63*, 12725−12747.
(15) Qiao, J.; Li, Y.-S.; Zeng, R.; Liu, F.-L.; Luo, R.-H.; Huang, C.; Wang, Y.-F.; Zhang, J.; Quan, B.; Shen, C.; Mao, X.; Liu, X.; Sun, W.; Yang, W.; Ni, X.; Wang, K.; Xu, L.; Duan, Z.-L.; Zou, Q.-C.; Zhang, H.-L.; Qu, W.; Long, Y.-H.-P.; Li, M.-H.; Yang, R.-C.; Liu, X.; You, J.;

Zhou, Y.; Yao, R.; Li, W.-P.; Liu, J.-M.; Chen, P.; Liu, Y.; Lin, G.-F.; Yang, X.; Zou, J.; Li, L.; Hu, Y.; Lu, G.-W.; Li, W.-M.; Wei, Y.-Q.; Zheng, Y.-T.; Lei, J.; Yang, S. SARS-CoV-2 M^{pro} inhibitors with antiviral activity in a transgenic mouse model. *Science* **2021**, *371*, 1374−1378.

(16) Schechter, I. Reprint of "on the size of the active site in proteases. I. Papain". *Biochem. Biophys. Res. Com.* **2012**, *425*, 497−502. . The nomenclature used is that of Schechter, I. and Berger, A., where the residues on the N-terminus side of the peptide bond that is cleaved are designated as P_1−P_n and those on the C-terminus side are designated P_1−P_1'. The corresponding active-site subsites are designated S_1−S_n and S_1−S_n'. S_1 is the primary substrate specificity subsite, and P_1−P_1' is the scissile bond

(17) Rathnayake, A. D.; Zheng, J.; Kim, Y.; Perera, K. D.; Mackin, S.; Meyerholz, D. K.; Kashipathy, M. M.; Battaile, K. P.; Lovell, S.; Perlman, S.; Groutas, W. C.; Chang, K.-O. 3C-like protease inhibitors block coronavirus replication in vitro and improve survival in MERS-CoV-infected mice. *Sci. Transl. Med.* **2020**, *12*, No. eabc5332.

(18) Kim, Y.; Liu, H.; Galasiti Kankanamalage, A. C.; Weerasekara, S.; Hua, D. H.; Groutas, W. C.; Chang, K.-O.; Pedersen, N. C. Reversal of the progression of fatal coronavirus infection in cats by a broad-spectrum coronavirus protease inhibitor. *PLoS Pathog.* **2016**, *12*, No. e1005531.

(19) Pedersen, N. C.; Kim, Y.; Liu, H.; Galasiti Kankanamalage, A. C.; Eckstrand, C.; Groutas, W. C.; Bannasch, M.; Meadows, J. M.; Chang, K.-O. Efficacy of a 3C-like protease inhibitor in treating various forms of acquired feline infectious peritonitis. *J. Feline Med. Surg.* **2018**, *20*, 378−392.

(20) Pirali, T.; Serafini, M.; Cargnin, S.; Genazzani, A. A. Applications of deuterium in medicinal chemistry. *J. Med. Chem.* **2019**, *62*, 5276−5297.

(21) Timmins, G. S. Deuterated drugs; updates and obviousness analysis. *Expert Opin. Ther. Pat.* **2017**, *27*, 1353−1361.

(22) Liu, J. F.; Harbeson, S. L.; Brummel, C. L.; Tung, R.; Silverman, R.; Doller, D. A decade of deuteration in medicinal chemistry. *Annu. Rep. Med. Chem.* **2017**, *50*, 519−542.

(23) Ghosh, A. K.; Doung, T. T.; McKee, S. P.; Thompson, W. J. N,N-dissuccinimidyl carbonate: a useful reagent for alkoxycarbonylation of amines. *Tetrahedron Lett.* **1992**, *33*, 2781−2784.

(24) Kjell, D. P.; Slattery, B. J.; Semo, M. J. A novel, nonaqueous method for regeneration of aldehydes from bisulfite adducts. *J. Org. Chem.* **1999**, *64*, 5722−5724.

(25) Kim, Y.; Lovell, S.; Tiew, K.-C.; Mandadapu, S. R.; Alliston, K. R.; Battaile, K. P.; Groutas, W. C.; Chang, K.-O. Broad-spectrum antivirals against 3C or 3C-like proteases of picornaviruses, noroviruses, and coronaviruses. *J. Virol.* **2012**, *86*, 11754−11762.

(26) Gampe, C.; Verma, V. A. Curse or cure? A perspective on the developability of aldehydes as active pharmaceutical ingredients. *J. Med. Chem.* **2020**, *63*, 14357−14381.

(27) Cargnin, S.; Serafini, M.; Pirali, T. A primer of deuterium in drug design. *Future Med. Chem.* **2019**, *11*, 2039−2042.

(28) Meanwell, N. A. Synopsis of some recent tactical application of bioisosteres in drug design. *J. Med. Chem.* **2011**, *54*, 2529−2591.

(29) Chessari, G.; Hardcastle, I. R.; Ahn, J. S.; Anil, B.; Anscombe, E.; Bawn, R. H.; Bevan, L. D.; Blackburn, T. J.; Buck, I.; Cano, C.; Carbain, B.; Castro, J.; Cons, B.; Cully, S. J.; Endicott, J. A.; Endicott, J. A.; Fazal, L.; Golding, B. T.; Griffin, R. J.; Haggerty, K.; Harnor, S. J.; Hearn, K.; Hobson, S.; Holvey, R. S.; Howard, S.; Jennings, C. E.; Johnson, C. N.; Lunec, J.; Miller, D. C.; Newell, D. R.; Noble, M. E. M.; Reeks, J.; Revill, C. H.; Riedinger, C.; Denis, J. D.; Tamanini, E.; Thomas, H.; Thompson, N. T.; Vinković, M.; Wedge, S. R.; Williams, P. A.; Wilsher, N. E.; Zhang, B.; Zhao, Y. Structure-based design of potent and orally active isoindolinone inhibitors of MDM2-p53 protein-protein interaction. *J. Med. Chem.* **2021**, *64*, 4071−4088.

(30) Kabsch, W. Automatic indexing of rotation diffraction patterns. *J. Appl. Crystallogr.* **1988**, *21*, 67−72.

(31) Kabsch, W. XDS. *Acta Crystallogr., Sect. D: Biol. Crystallogr.* **2010**, *66*, 125−132.

(32) Vonrhein, C.; Flensburg, C.; Keller, P.; Sharff, A.; Smart, O.; Paciorek, W.; Womack, T.; Bricogne, G. Data processing and analysis with theautoPROCtoolbox. *Acta Crystallogr., Sect. D: Biol. Crystallogr.* **2011**, *67*, 293−302.

(33) Evans, P. R. An introduction to data reduction: space-group determination, scaling and intensity statistics. *Acta Crystallogr., Sect. D: Biol. Crystallogr.* **2011**, *67*, 282−292.

(34) McCoy, A. J.; Grosse-Kunstleve, R. W.; Adams, P. D.; Winn, M. D.; Storoni, L. C.; Read, R. J. Phasercrystallographic software. *J. Appl. Crystallogr.* **2007**, *40*, 658−674.

(35) Adams, P. D.; Afonine, P. V.; Bunkóczi, G.; Chen, V. B.; Davis, I. W.; Echols, N.; Headd, J. J.; Hung, L.-W.; Kapral, G. J.; Grosse-Kunstleve, R. W.; McCoy, A. J.; Moriarty, N. W.; Oeffner, R.; Read, R. J.; Richardson, D. C.; Richardson, J. S.; Terwilliger, T. C.; Zwart, P. H. PHENIX: a comprehensive Python-based system for macromolecular structure solution. *Acta Crystallogr., Sect. D: Biol. Crystallogr.* **2010**, *66*, 213−221.

(36) Emsley, P.; Lohkamp, B.; Scott, W. G.; Cowtan, K. Features and development ofCoot. *Acta Crystallogr., Sect. D: Biol. Crystallogr.* **2010**, *66*, 486−501.

(37) Chen, V. B.; Arendall, W. B.; Headd, J. J.; Keedy, D. A.; Immormino, R. M.; Kapral, G. J.; Murray, L. W.; Richardson, J. S.; Richardson, D. C. MolProbity: all-atom structure validation for macromolecular crystallography. *Acta Crystallogr., Sect. D: Biol. Crystallogr.* **2010**, *66*, 12−21.

(38) Potterton, L.; McNicholas, S.; Krissinel, E.; Gruber, J.; Cowtan, K.; Emsley, P.; Murshudov, G. N.; Cohen, S.; Perrakis, A.; Noble, M. Developments in theCCP4 molecular-graphics project. *Acta Crystallogr., Sect. D: Biol. Crystallogr.* **2004**, *60*, 2288−2294.

(39) Evans, P. Scaling and assessment of data quality. *Acta Crystallogr., Sect. D: Biol. Crystallogr.* **2006**, *62*, 72−82.

(40) Diederichs, K.; Karplus, P. A. Improved R-factors for diffraction data analysis in macromolecular crystallography. *Nat. Struct. Biol.* **1997**, *4*, 269−275.

(41) Weiss, M. S. Global indicators of X-ray data quality. *J. Appl. Crystallogr.* **2001**, *34*, 130−135.

(42) Karplus, P. A.; Diederichs, K. Linking crystallographic model and data quality. *Science* **2012**, *336*, 1030−1033.

(43) Evans, P. Resolving Some Old Problems in Protein Crystallography. *Science* **2012**, *336*, 986−987.

https://doi.org/10.1021/acs.jmedchem.1c00319
J. Med. Chem. XXXX, XXX, XXX−XXX